Master's thesis

NTNU
Norwegian University of Science and Technology
Faculty of Natural Sciences
Department of Chemistry

Peder Langsholt Holmqvist

NON-ISOTHERMAL TRANSPORT IN CATION-EXCHANGE MEMBRANES

The Seebeck effect in systems of ions abundant in seawater

Master's thesis in Chemical Engineering and Biotechnology
Supervisor: Signe Kjelstrup
June 2020

NTNU
Norwegian University of
Science and Technology

Peder Langsholt Holmqvist

NON-ISOTHERMAL TRANSPORT IN CATION-EXCHANGE MEMBRANES

The Seebeck effect in systems of ions abundant in seawater

Master's thesis in Chemical Engineering and Biotechnology
Supervisor: Signe Kjelstrup
Co-supervisor: Kim Roger Kristiansen
June 2020

Norwegian University of Science and Technology
Faculty of Natural Sciences
Department of Chemistry

NTNU
Norwegian University of
Science and Technology

Abstract

In this thesis, the Seebeck effect in ion-exchange membranes relevant for reverse electrodialysis (RED) has been measured. The Seebeck effect is an electric potential gradient due to a temperature gradient, and was measured with solutions of ions abundant in seawater. The motivation for this is to better understand how RED can be combined with waste-heat harvesting for increased power production.

The thermoelectric potential has previously been measured in membranes in equilibrium with single-salt solutions, and most extensively with NaCl and KCl. In this thesis, the Seebeck coefficient in Fumasep FKS-75 μm membranes was measured in single-salt solutions of NaCl, KCl, $MgCl_2$ and $CaCl_2$, as well as in binary NaCl$-$$MgCl_2$ solutions and in a sample of seawater. In the single-salt solutions, a relation between the Seebeck coefficient and the hydrated radius of the ions was found. In the binary NaCl$-$$MgCl_2$ systems, even small amounts of Mg^{2+} had relatively large, negative effects on the Seebeck coefficient. Two different methods of analysis indicated that this was due to a high fraction of Mg^{2+} in the membrane. The thermoelectric potential was also measured with a seawater sample, where the Seebeck coefficient was measured to be higher than with pure NaCl at the same total ion concentration. This is contradictory to what we would expect from the NaCl$-$$MgCl_2$ systems, and from Mg^{2+} being the second-most abundant cation in seawater. This result is yet to be satisfactorily explained, and mixed electrolytes with Ca^{2+} and K^+ should be investigated.

Currently, the ion-exchange membrane is a limiting factor in the economical feasibility of salt power production from RED. Development and characterization of new membranes is therefore of huge interest. The thermoelectric potential in novel, cellulose-based membranes has been measured. The results from these measurements were inconclusive, however.

In the thermoelectric potential measurements, the temperature gradient across the membrane stack is sustained by circulating solutions at different temperatures on each side of the membranes. The temperatures were measured in the bulk solutions, which are different from the membrane surface temperatures if there are temperature gradients in the solution. The emergence of temperature gradients between the bulk solution and the membrane surfaces is known as temperature polarization. The effect of temperature po-

larization was here investigated using computational fluid dynamics (CFD). The software ANSYS Fluent 2019 R3 was used to model the flow and heat-transfer in the experimental setup. The simulations showed that temperature polarization indeed was present, and that the temperature difference across the stack of membranes was approximately 88% of the temperature difference between the bulk solutions.

Sammendrag

I denne masteroppgaven har seebeckeffekten blitt målt i ionebyttermembraner som er relevante for revers elektrodialyse (RED). Seebeckeffekten er elektrisk spenning som oppstår som følge av en temperaturgradient, og hensikten her er å undersøke denne effekten, for potensielt å øke elektrisitetsproduksjonen i RED ved å utnytte industriell spillvarme.

Det termoelektriske potensialet har tidligere blitt målt i membraner i likevekt med enkeltsaltløsninger, og mest omfattende med NaCl og KCl. I denne avhandlingen ble Seebeckkoeffisienten i Fumasep FKS-75 μm-membraner målt med enkeltsaltløsninger av NaCl, KCl, $MgCl_2$ og $CaCl_2$, i tillegg til binære NaCl$-$$MgCl_2$-løsninger og en prøve av sjøvann. I enkeltsaltløsningene ble det funnet en sammenheng mellom Seebeck-koeffisienten og radien til de hydrerte ionene. I de binære NaCl$-$$MgCl_2$-systemene hadde selv små mengder Mg^{2+} en relativt stor og negativ innvirkning på Seebeck-koeffisienten. To forskjellige analysemetoder indikerte at dette skyldtes at transporttallet til magnesium i membranen var høyt relativt til konsentrasjonen i løsningen.

Det termoelektriske potensialet ble også målt i membraner i likevekt med en sjøvann, hvor Seebeck-koeffisienten ble målt til å være høyere enn med ren NaCl med samme totale saltkonsentrasjon. Dette er motstridende med hva vi kan forvente utfra resultatene fra de binære NaCl$-$$MgCl_2$-systemene, og med tanke på at Mg^{2+} er kationet med nest høyest konsentrasjon i sjøvann. Dette resultatet mangler en tilfredsstillende forklaring, men en grunn kan være forekomst av andre ioner, spesielt K^+, som man kan forvente at har en positiv effekt på Seebeckkoeffisienten.

Ionebyttermembranen er en begrensende faktor for at RED skal være økonomisk lønnsomt. Utvikling og karakterisering av nye membraner er derfor viktig for denne teknologien. Det termoelektriske potensialet i nye, cellulosebaserte membraner er målt. Resultatene fra disse målingene tyder imidlertid på at temperaturpolarisering hadde stor innvirkning, og at ionebyttermembranene hadde begrenset innvirkning på det målte potensialet.

I målingene som ble gjort av det termoelektriske potensialet, ble en temperaturgradient over membranene opprettholdt ved å sirkulere løsninger på hver side av membranene. Temperaturforskjellen ble målt i bulkløsningen, som vil være forskjellig fra temperaturforskjellen over membranen dersom det oppstår temperaturgradienter i løsningen. Dette

fenomenet kalles temperaturpolarisering, og ble her undersøkt med fluidmekansike beregninger. Temperaturen på membranoverflaten ble estimert ved å bruke programvaren ANSYS Fluent 2019 R3 for å modellere væskestrømmene gjennom termocellen, og temperaturforskjellen over membranen ble estimert å være 88% av den målte temperaturforskjellen.

Acknowledgements

First of all, I thank my supervisor Signe Kjelstrup for including me in the research group, for patient supervision and guidance, and my co-supervisor Kim R. Kristiansen for his supervision, and for help with the laboratory work, not least for the experiments coducted while the campus was shut down for students.

This semester has taken some unexpected twists due to the pandemic and campus shut-down, which has also affected this thesis. One consequence of this is the inclusion of a CFD analysis of the experimental setup, which did not require any physical attendance on campus. I thank Associate prof. Kristian Etienne Einarsrud for valuable advice on implementation of the fluid simulations.

Lastly, I thank my fellow classmates for the lunch- and coffee breaks, for joyous discussions and simply creating a delightful workning environment.

Contents

Chapter 1

Introduction

Reverse electrodialysis (RED) is a technology to produce electricity from the process of mixing solutions of different salinity, such as fresh- and seawater. While not yet commercialized, the technology is currently subject to pilot testing [1]. Electricity is produced by allowing the mixing to occur through ion-exchange membranes (IEMs), which are membranes permeable to either cations or anions. While the concentration gradients across the membranes are driving the ion transport in conventional RED, an electric potential gradient can also develop when a temperature gradient is applied across the membranes. The emergence of this thermoelectric potential is the Seebeck effect, and could be exploited to increase the power-output in RED [2]. Chapter 2 gives an introduction to conventional RED, and recent development of technologies combining RED and waste-heat harvesting. The IEM is fundamental in RED, and an important part of the research related to RED is the development of new IEMs, and the chapter will also cover this briefly.

Thermoelectric potential measurements of a RED unit cell operated with realistic fresh- and seawater samples yielded a higher thermoelectric potential than what one would expect from pure NaCl solutions [2]. This motivates the main goal of this thesis, namely to investigate how different ion species, and mixtures of ions affect the membrane's contribution to the Seebeck effect. In this thesis, the thermoelectric potential is measured in single-salt solutions of NaCl, KCl, $MgCl_2$ and $CaCl_2$, as well as in binary $NaCl-MgCl_2$ solutions and in one seawater sample. Expressions for the thermoelectric potential valid for solutions of mixed chloride salts are derived, as well as data reduction procedures to interpret the results. This work is presented in chapter 4. The chapter will also present thermoelectric potential measurements in novel, cellulose-based membranes.

The measurements in chapter 4 are carried out in a cell where a stack of membranes is placed between two chambers with solutions at different temperatures. This could lead to temperature gradients between the bulk solutions and the membrane surfaces, affecting the measured thermoelectric potential. In chapter 3, this issue is addressed by simulating the heat transfer between the solutions and membranes with computational fluid dynamics (CFD).

Chapter 2

RED and waste-heat harvesting

2.1 Power production from salinity gradients

When fresh- and saltwater is mixed, the free energy of mixing can be exploited for power production. This is done by allowing the mixing to occur through membranes. There are two main technologies for this. One is to use membranes permeable to water, where water is transported from the dilute to the saline solution, causing a pressure gradient to build up. This is pressure retarded osmosis (PRO) [3]. The other technology is reverse electrodialysis (RED) where membranes permeable to the positive and negative ions respectively, are utilized to allow mixing. This thesis will focus on enhancing the latter technology.

2.1.1 Conventional RED

RED is a technology to produce electricity from the mixing of solutions with different salinity. By only allowing mixing to occur through ion-exchange membranes, the process results in a net transport of charge. This is visualized in figure 2.1. This figure shows the overall process of RED: Cations are transported from the concentrate to the dilute stream through a cation exchange membrane (CEM), while only anions will permeate through the anion-exchange membrane (AEM) from the right-hand side. The electrodes are closing the circuit. To increase the power output, this structure can be repeated to form a stack of alternating layers of dilute and concentrated streams separated by CEMs and AEMs. The RED technology has been subject to extensive research in the last decades, we refer to e.g. Tang [4] for a recent review.

2.1.2 Effect of multivalent ions in RED

The most abundant ions in sea- and brackish water are Na^+ and Cl^-, but also ions such as Mg^{2+}, Ca^{2+}, K^+ and $SO_4{}^{2-}$ are present in significant amounts and may have a large effect on the RED performance when harvesting salinity gradient energy. Two effects of multivalent ions have been reported by several, namely increased membrane resistance,

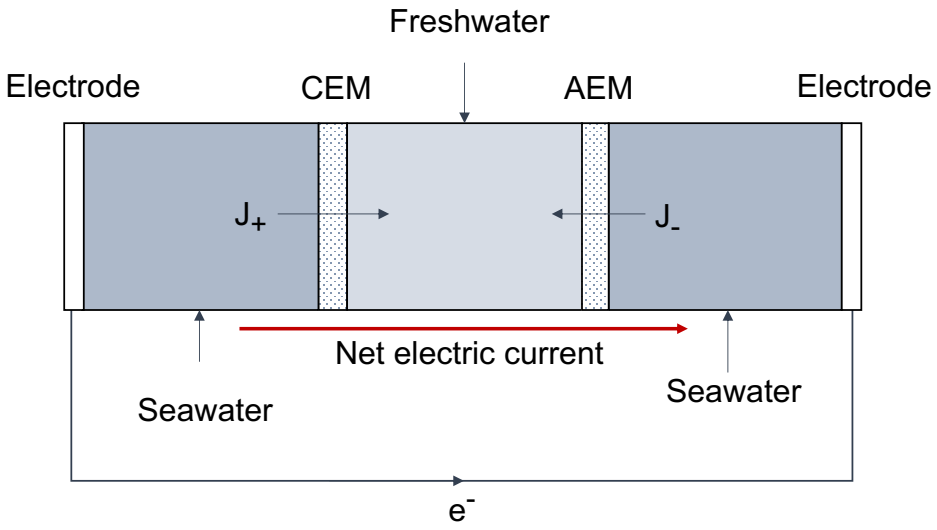

Figure 2.1: Schematic representation of a RED unit cell with natural feed streams. A flux of cations permeates from the seawater on the left-hand side to the dilute stream, while the AEM only allows anions to permeate from the stream on the right-hand side. The electrodes are connected through an external circuit, allowing the net current to be harvested for power production.

and uphill transport of the multivalent ions [5–8]. Uphill transport is transport against the ion's concentration gradient. The uphill transport occurs when the monovalent ions are transported through the IEM, along the concentration gradient. To obey electroneutrality, an uphill transport of multivalent ions occurs and reduces the net electric current. Vermaas et. al. [7] reports a 29 - 50 % decrease in the RED power density when 10% $MgSO_4$ is added to NaCl feed solutions. One approach that inhibits the uphill transport is to use either monovalent- or multivalent selective membranes [6].

2.1.3 RED coupled with waste-heat harvesting

Power production from RED can be enhanced by coupling the process with a heat source. This can be done by creating a temperature gradient between the feed solutions and thus utilize the thermoelectric potentials of the IEMs, but there are other ways to couple heat harvesting and RED. In a sense, this is always the case when river- and seawater is mixed, with the sun being the heat source that drives the natural water cycle and sustains the salinity gradients. This occurs on a more local form in a RED pilot plant in Sicily, Italy [1], which has been run using brackish water and brine, the brine being naturally regenerated by evaporation while it is stored in open basins. More technologically advanced concepts have been developed within the EU-funded RED-heat-to-power project: One is coupling of RED and membrane distillation [9] in a closed-loop system. Here, waste heat is driving a membrane distillation process that regenerates the salinity gradient. Another is a closed-loop concept with NH_4CO_3, where solutions are regenerated by heating such that NH_4CO_3 decomposes [10, 11]. This concept has been subject to lab-scale pilot testing.

These concepts, however, do not utilize the thermoelectric properties of the ion-exchange membrane. There have been conducted studies on temperature gradients in electrodialysis under driving currents [12]. In these studies, the largest increases in power output were observed when both streams are heated, due to lower cell resistance.

2.2 Thermoelectric potential in IEMs

The thermoelectric potential in ion-exchange membranes has been a field of research since the beginning of the 20th century, and Lakshminarayanaiah [13] sums up the early research on the subject. Notable work has been done by Tasaka and coworkers [14, 15]. Their results show a consistent linear dependence between the thermoelectric potential and the electrolyte activity for various electrolytes. Scibona et. al. [16] measured the thermoelectric potential of Nafion membranes in solutions of LiCl, NaCl, KCl, and CsCl. Barragán et. al. [17] gave a systematic review of thermoelectric potential measured in the literature, in the framework of non-equilibrium thermodynamics. There have been recent studies modeling the thermoelectric effects in electrolytes in porous materials [18–20], while remarkably large Seebeck coefficient has been reported in a system with oxidized and aligned cellulose membranes [21]. Coupling of the thermoelectric potential of ion exchange membranes and RED has also been investigated [2], suggesting that the cell potential could be increased with 1.3% per Kelvin of temperature difference across the membrane in a sea-brackish water system.

2.3 The ion exchange membrane

2.3.1 Membrane characteristics

The key component in the RED technology is the ion exchange membrane, and the cost of membranes is a limiting factor for the technology to be economically feasible. The technology is dependent on membranes with improved properties, produced at reduced costs compared with the current commercial membranes [22]. A summary of important characteristics determining the performance of ion-exchange membranes is given below.

The selectivity can be measured in terms of the ion transport number, which is the fraction of the electric current that is carried by the cation in a cation exchange membrane and the fraction that is carried by the anion in an anion exchange membrane. The selectivity should be as high as possible. In systems of multiple ions, the selectivity towards specific ions is relevant, this can be done by surface modification of the membranes [23]. Monovalent-selective cation exchange membranes are for example prepared by adding a thin layer of cationic charge sites at the surface of the otherwise negatively charged membrane [24]. A recent review of research on selectivity in ion-exchange membranes is given by Luo et al [25].

Ion exchange capacity (IEC) is a measure of the number of fixed charge groups in the dry membrane. A high IEC is beneficial, both because this gives higher electric conductivity, and because the selectivity increases when the density of fixed charges is high, relative to the electrolyte concentration [25]. The effect is however counteracted by an increased degree of swelling which usually is correlated with the IEC, and which lowers the selectivity [4]. A high IEC with limited swelling is therefore optimal. The IEC of commercial IEMs is typically in the range of 1-3 mEq/g [4].

Low electric resistance is beneficial in RED, so the counter-ions can easily permeate through the membrane. The electric resistance of commercial membranes in NaCl solutions are typically in the range of 1-10 Ω cm^{-2} [26], and typically increases with presence of divalent ions [5, 6].

In RED coupled with waste-heat harvesting, low thermal conductivity is beneficial to sustain a temperature gradient over the membrane. A high thermoelectric effect is obtained when the heat is transported by the ions instead of through thermal conduction. In Nafion membranes, the thermal conductivity is increasing with the water content and has been measured to be 0.25 W/m K in fully wetted membranes [27].

2.3.2 Development of new ion-exchange membranes

Most commonly used commercial IEMs such as Nafion membranes are perfluorinated membranes with high production costs. Avci et. al. [28] have recently developed an polyethersulfone-based IEM for RED, which performed comparable and better than current commercial membranes when using brine and brackish water. Liu et. al. [29] have fabricated a nanoporous carbon membrane yielding a maximum power density output almost two orders of magnitude larger than the power density in currently available membranes. This is attributed to its high ionic conductivity. A class of interesting membranes is membranes made from biopolymers, due to environmental concerns, and potentially lower production costs. Cellulose, chitosan, and alginate are three biopolymers that have been subject to research for ion-exchange membrane applications [30–32]. Yee et al. [33] reviewed the development of new membrane types and concluded that membranes from non-fluorinated materials such as poly-aryl ethers, polysulfones, and cellulose-derived materials could be competitive alternatives to the current commercial options.

Chapter 3

Computational fluid dynamics analysis of temperature polarization

Temperature polarization is the phenomenon of temperature gradients in the feed solutions and is potentially a source of error in the experiments, as the temperature difference across the membrane would be different from the bulk temperature difference [34]. The effect can be minimized by increasing the membrane thickness [2] or increasing the solution stirring rate [35]. The effect can also be evaluated using computational fluid dynamics (CFD). The flow chamber used in the experimental section of this thesis will here be modelled as a heat exchange problem. The cell consists of two chambers separated by a membrane, and in the two chambers, water flows at different temperatures. When the temperature and electric potential difference are measured in the bulk solutions, this will be equal to the temperature and potential difference across the membrane only if the temperature polarization is negligible. We will here use the computational fluid dynamics software ANSYS Fluent 2019 R3 to model the temperature polarization, using methods well-known for modelling conjugate heat transfer.

3.1 CFD - general theory

Computational fluid dynamics is the field of study concerned with using computational methods to evaluate the transport of fluids. Fluid transfer is governed by the Navier Stokes equations that can be solved only for simple geometries in special cases. The computational methods to solve general flow problems involve spatial and temporal discretization methods, iteration schemes and, if the flow is turbulent, the use of turbulence models. An overview of different topics relevant to this work will be given below.

Governing equations

All fluid flows are governed by the conservation of mass and momentum. When heat transfer is present, the energy equation must be included. The conservation equation for the mass can be expressed as

$$\frac{\partial \rho}{\partial t} = -\nabla \cdot (\rho v) \tag{3.1}$$

where ρ is the fluid density, and v is the velocity vector. The the momentum conservation equation can be written as [36]

$$\frac{\partial}{\partial t}(\rho v) + \nabla \cdot (\rho v v) = -\nabla p + \nabla \cdot \tau^s + \rho g + F_b \tag{3.2}$$

Where p is the pressure, τ^s is the shear stress tensor, g is the gravitational acceleration and F_b is other body forces. When heat transfer is present, the Ansys fluent software includes the energy equation in the form [36]:

$$\frac{\partial}{\partial t}(\rho E) + \nabla \cdot (v(\rho E + p)) = \nabla \cdot (k_{\text{eff}} \nabla T - \sum_j h_j J_j + (\tau^s_{\text{eff}} \cdot v)) + S_h \tag{3.3}$$

Where E is the specific energy, k_{eff} and τ^s_{eff} is the effective thermal conductivity and stress tensor determined by the turbulence conditions, h_j and J_j is the enthalpy and diffusion flux of species j, and S_h is other energy source terms. These three equations are valid for compressible fluids. However, they may be simplified when the fluid is incompressible and the density can be regarded as constant. These equations can only be solved analytically in special cases for simple geometries. An overview over relevant models and computational methods provided by the ANSYS Fluent software to solve these equations is given below.

Spatial discretization

The ANSYS Fluent solver is based on the finite volume method. That is, the flow domain is divided into discrete control volumes, and the model equations are computed in the centre of each of these volumes [37]. The spatially discretized domain is called the mesh grid. The meshgrid can be either unstructured or structured and consist of either tetrahedral or hexahedral elements. While a structured mesh of hexahedral elements will be less computationally expensive than a comparable mesh of tetrahedral elements, tetrahedral elements are more flexible when constructing a mesh of a complex geometry [37]. The Ansys software also allows the mesh to consist of both types, using tetrahedral elements in areas where the geometry is complex, and hexahedral elements elsewhere. Poor quality of the mesh can have negative effects on convergence and the quality of the simulation. A commonly used quality metric is the cell skewness, and the mesh should have a maximum skewness below 0.95 and an average below 0.33 [38].

Turbulence models

Turbulent flows are characterized by random fluctuations from the mean velocity and will develop as a fluid flows along a wall or is otherwise subject to obstacles. Turbulent flows can be resolved numerically by solving the time-dependent Navier-Stokes equations without approximations, but this is computationally extremely expensive, and a more feasible approach is to use some approximative model [37]. One class of models is the Reynolds-averaged Navier Stokes models (RANS-models). These methods rely on using a time average of the continuity, momentum, and energy equations and evaluate the turbulence in terms of the average of fluctuations from the mean velocity, rather than the

single fluctuations. While there exist a number of different methods, a commonly used class of models are the k-ϵ models, with the standard, RNG, and realizable models being available in the Ansys Fluent software. In the k-ϵ models, the turbulence is evaluated using two additional equations for k, the turbulent kinetic energy, and ϵ, the turbulent energy dissipation rate [37]. The RNG k-ϵ model is modified using renormalization group theory (RNG) and is suitable for a wider range of flows than the standard k-ϵ model, such as strained flows and for realizing flows in the near-wall region [36]. The near-wall region is defined in terms of the dimensionless wall distance $y+ = yu_\tau/\nu$ [37], where y is the distance from the wall, ν is the kinematic viscosity and $u_\tau = \sqrt{\tau\rho}$, is the friction velocity. When realizing flows in near-wall modelling, the grid should be refined such that the center of the cells adjacent to the wall gives a $y+$ not larger than of $O(1)$ [36].

Heat transfer

To generalize the results from the CFD simulations, a simple heat transfer model is proposed. According to Fourier's law of conduction, the heat flux through the membrane is

$$J'_q = -k_m \frac{\Delta_m T}{l_m} \tag{3.4}$$

where k_m is the thermal conductivity of the membrane, l_m is the membrane thickness, and $\Delta_m T$ is the temperature difference across the membrane. In turbulent flow conditions, forced convection governs the heat transfer, and the temperature boundary layer can be assumed to be only dependent on the Reynolds number, i.e. the flow conditions. The heat transfer from the membrane surface to the bulk can be expressed for some heat transfer coefficient h as

$$J'_q = -h\Delta_\delta T \tag{3.5}$$

Where $\Delta_\delta T$ is the temperature difference in the boundary layer between the bulk and the membrane surface. We write the bulk difference as $\Delta_{1,2}T$, and the temperature differences across the boundary layers become $\Delta_\delta T = \frac{1}{2}(\Delta_{1,2}T - \Delta_m T)$. At steady state conditions, the heat flux through the membrane is equal to the heat flux through the boundary layer. In turbulent flow and moderate temperature differences, we may assume that the thermal boundary layer is dependent on the flow instead of the temperature gradient between the surface and the bulk. Using this we expect the temperature difference across the membrane to be proportional to the bulk temperature difference. Combining the heat transfer equations, we can write the temperature difference across the membrane as

$$\Delta_m T = \frac{h}{h + \frac{2k_m}{l_m}} \Delta_{1,2} T \tag{3.6}$$

$$= \frac{1}{1 + \frac{2k_m}{hl_m}} \Delta_{1,2} T \tag{3.7}$$

$$= c\Delta_{1,2} T \tag{3.8}$$

Where the assumption that h is constant with the temperature is equivalent to the assumption that heat transfer in the solution is governed by the flow conditions. While

this will not be done here, the equation can be rewritten to find h and then estimate the membrane surface temperature as a function of the membrane thickness.

3.2 Model and simulation

A 3D model of the flow chambers was created in Solidworks and with the Ansys software (models are shown in appendix A). A full model of the flow chambers and the membrane was assembled in Ansys designmodeler, and converted into a mesh using the Ansys meshing tool. The meshed version of the model can be viewed in figure 3.1. A combination of tetrahedral and hexahedral cells was used to ensure a good quality of all cell volumes while reducing computational time by using hexahedral cells where appropriate. Figure 3.1 shows where the mesh is partitioned in hexahedral and tetrahedral cells. Moreover, inflation layers with a first-layer thickness of 50 μm were used at the membrane surface to capture the boundary layer along the membrane, and to ensure $y+$ values below 1. Model sizing was employed such that the cell quality was kept satisfactory. The maximum cell skewness of the mesh was 0.8, with an average of 0.2. The membrane mesh was sized such that it was dived into 100 cells in the membrane thickness direction. The final model consisted of 4 670 000 elements.

Ansys Fluent 2019 R3 with double precision was used to perform the simulations. The steady-state, pressure-based solver was employed. Water with properties from the Ansys fluent database, at a reference temperature of 300 K, was used as the fluid medium, with material properties independent of the temperature. For the thermal conductivity of the membrane, 0.25 W/m was used, which is measured in fully wetted Nafion membranes [27]. The inlet velocity was set to 1.11 m/s, corresponding to a pump velocity of 17 L/min, the pump velocity of Grant Ecocool 100, which is used in the experimental section of this thesis. Hydraulic diameter and turbulence intensity were specified to 0.009 m (equal to the inlet tube diameter) and 5% respectively. The turbulence model used was RNG k-ϵ with enhanced wall treatment. This model has been used by others [39, 40] in heat-transfer problems with comparable flow conditions. The solver settings were set to Green-Gauss node based spatial discretization, and the coupled solver with second-order upwind schemes for mass and momentum, and first-order upwind schemes for kinetic energy and turbulent dissipation.

To monitor the solution, the area-weighted average temperature at the membrane-fluid interfaces was used as a monitoring parameter in addition to the residuals. The solutions were iterated until the average temperatures remained constant within 4 decimals, typically after 400 iterations.

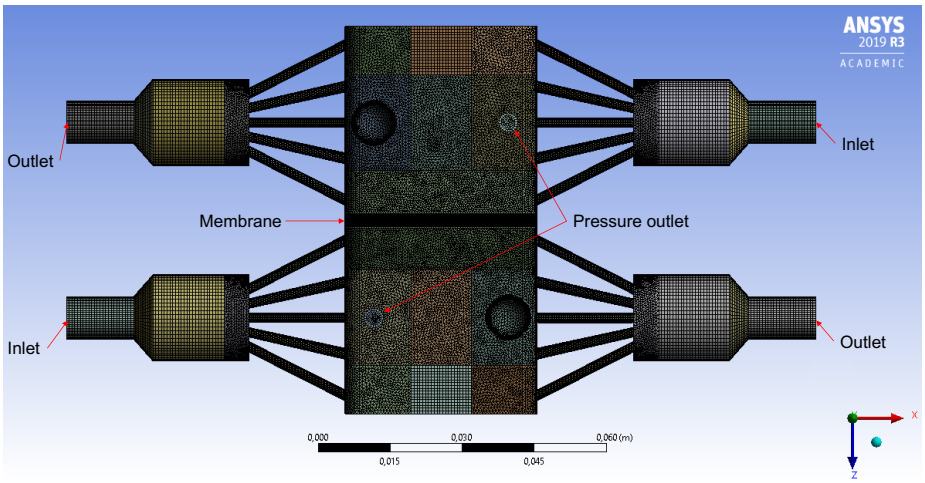

(a) Top view

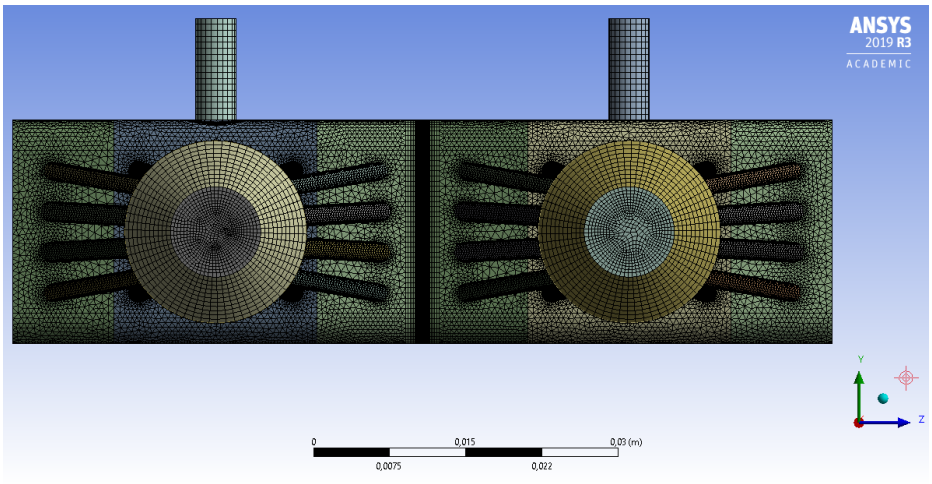

(b) Front view

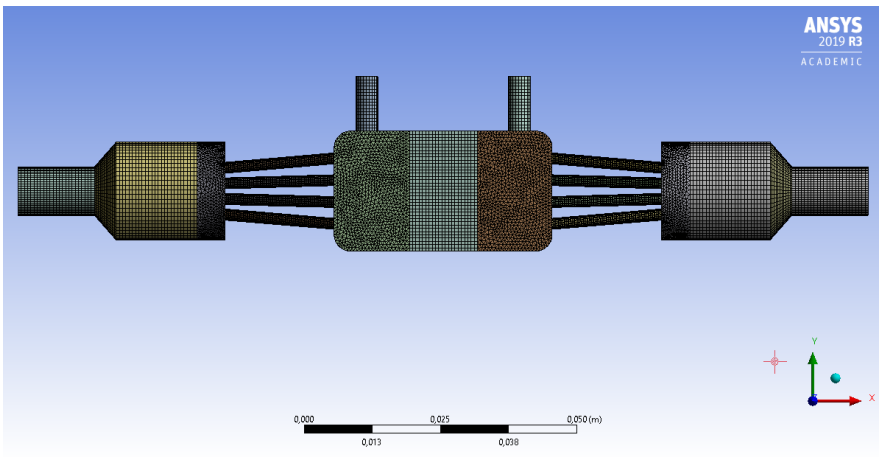

(c) Side view

Figure 3.1: The mesh used in CFD calculations, shown from above, front and the side. Inlets, outlets and the membrane are specified in the top view.

3.3 Results from CFD simulations

3.3.1 Mesh refinement test

To ensure that the simulation results were independent of the mesh (i.e. that the model is sufficiently refined), a mesh refinement test was done by refining the model such that the number of mesh elements was 9 800 000, approximately the double of the model to be used in the simulations. The area-weighted temperature difference across the membrane was estimated when the temperature difference across the membrane was 20 K. There was a deviation of 0.05 K from the temperature difference calculated with the original model. This was taken as acceptable, due to the computational costs of using a more refined model, compared with the expected gain in accuracy.

3.3.2 Membrane surface temperature

Figure 3.2 shows the temperatures at the membrane when the bulk temperatures are 308 and 288 K, respectively. The surface temperatures vary from temperatures close to the bulk temperature in the areas most exposed to the inlet flow, to approximately 3 K below or above the bulk temperature in areas of the membranes less exposed. The heat-transfer is thus not uniform, which could affect measurements of the thermoelectric potentials. However, the counter-current flow design reduces the variation in the temperature difference compared to a co-current flow design. The temperature contours of the two surfaces are inverted but otherwise close to identical. This is expected, as the two flow-chambers are identical.

The area-weighted temperature of the surfaces was recorded while the bulk temperatures were varied. Figure 3.3 shows the difference in the area-weighted surface temperatures plotted against the bulk temperature difference. The plot shows a linear relation, and we can relate the two quantities by the equation

$$\Delta_{\mathrm{m}}T = c\Delta_{1,2}T \tag{3.9}$$

Where c is a constant fraction of the bulk temperature difference. c was found from the slope in figure 3.3 and found to be 0.877 $\pm$0.003. As there was 0.05 K deviation between the temperature difference found with the original and refined model at $\Delta_{1,2}T = 20$, the true error in the temperature difference is at least that. To reflect this, the error in c is estimated from an error of 0.1 K in the temperature difference at 20 K.

The results can be compared with the evaluation of temperature polarization by Kristiansen et al. [2], for the same thermocell as used here. The Seebeck coefficient was measured as a function of the membrane stack thickness, and an expression where $c = \frac{1}{1+1/(l_m\rho)}$ was derived, with ρ as a fitting parameter. They found that $\rho = 0.004$ μm. That corresponds to $c = 0.75$, which is significantly lower than obtained here, indicating that

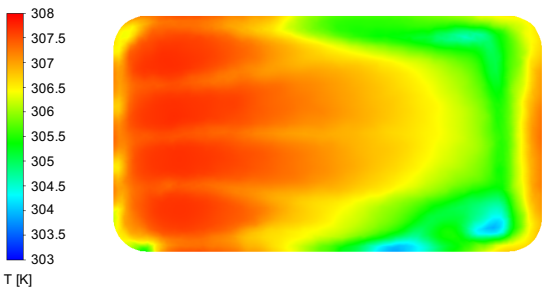

(a) Membrane surface temperature with bulk temperature at 308 K.

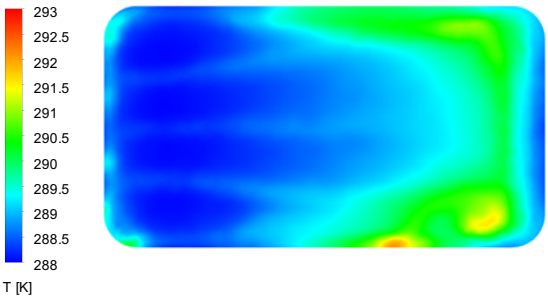

(b) Membrane surface temperature with bulk temperature at 288 K.

Figure 3.2: Contours of the temperature at the membrane surfaces adjacent to the hot and the cold solution, respectively, when the bulk temperature difference is 20 K.

temperature polarization plays a larger role. The deviation could be due to errors in resolving the temperature boundary layer due to the choice of turbulence model, or inaccuracies in the model of the flow-chamber. If we neglect these errors, however, we can investigate the effect of the membrane thermal conductivity. Combining equation (3.8) with the fitting parameter ρ we have that

$$\frac{1}{l_m \rho} = \frac{2k_m}{l_m h} \tag{3.10}$$

$$\implies k_m = \frac{h}{2\rho} \tag{3.11}$$

In the simulations, $k_m = 0.25$ W/m K, which combined with $c = 0.877$ gives $h = 4730\text{W/m}^2$ K. Now, h and $\rho = 0.004$ μm can be used in equation 3.11 and calculate the thermal conductivity of the membrane. This gives $k_m = 0.59$ W/m K. This is close to the thermal conductivity of water at 0.61 W/m K [41]. This is much higher than what has been measured in the Nafion membranes, and is possibly affected by a high water content in the membranes. To determine whether this high conductivity is due to modelling errors, it should be measured experimentally.

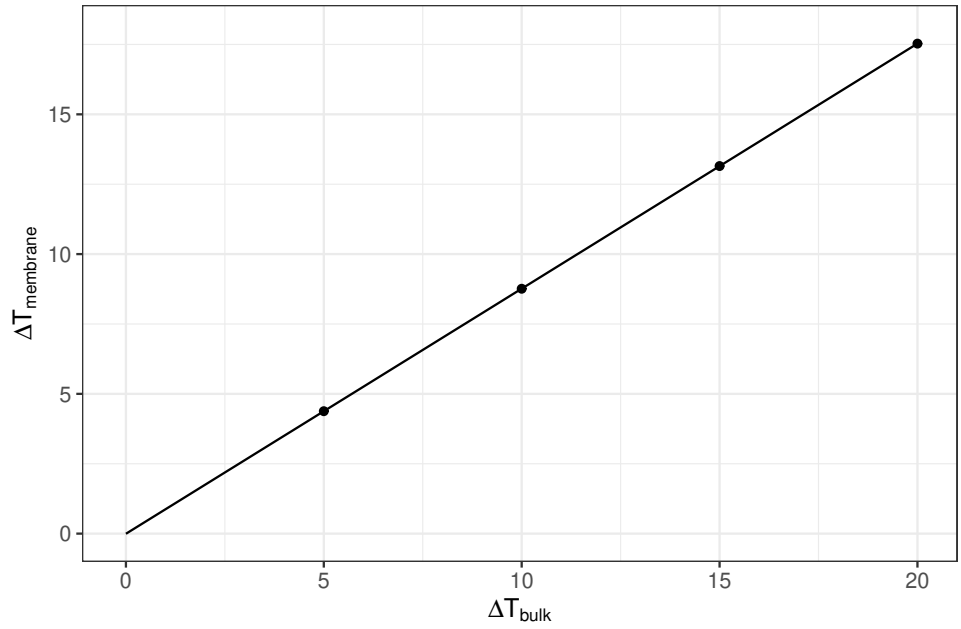

Figure 3.3: Temperature difference across the membrane plotted against the bulk temperature difference, for a membrane with a thickness of 750 μm. The temperature difference across the membrane is calculated from the area-weighted average temperature of the membrane surfaces.

Chapter 4

Thermoelectric potential in cation-exchange membranes

4.1 Theory

4.1.1 Thermoelectric potential in a solution with two chloride salts

The thermoelectric potential has previously been derived for single-salt solutions in the framework of nonequilibrium thermodynamics [2, 17]. In the following sections, the equations will be extended to mixtures of chloride salts, specifically for a mixture of NaCl and $MgCl_2$. The theory and notation here follows [42] and [43]. As experiments with single-salt solutions also are conducted in this thesis, single-salt equations will also be presented. Lastly, data reduction procedures for the purpose of analyzing experimental data will be derived.

We will consider contributions from the membrane, solution, electrode surfaces and the external circuit. We consider two compartments divided by an ion exchange membrane. Each compartment is filled with a solution of salt chlorides. The solutions have identical composition, but different temperatures. The position index of the left interface, adjacent to compartment 1 is denoted l. The position index on the right interface is denoted r. The notation Δ_m refers to the difference across the membrane, i.e. from l to r. The distinction between the bulk and the interfaces are included to account for possible temperature polarization in the solutions. A model of the system is shown in figure 4.1.

The membrane

We have transport of ions, heat and water through the membrane. We treat the membrane as a surface, and the entropy production through the membrane, σ_m can be expressed as:

$$\sigma_m = J_q'^{(r)} \Delta_m \left(\frac{1}{T}\right) - J_w \frac{\Delta_m \mu_w(T_l)}{T_l} - \sum_{\mathrm{MCl}_z} J_{\mathrm{MCl}_z} \frac{\Delta_m \mu_{\mathrm{MCl}_z}(T_l)}{T_l} - j \frac{\Delta_m \phi}{T_l} \tag{4.1}$$

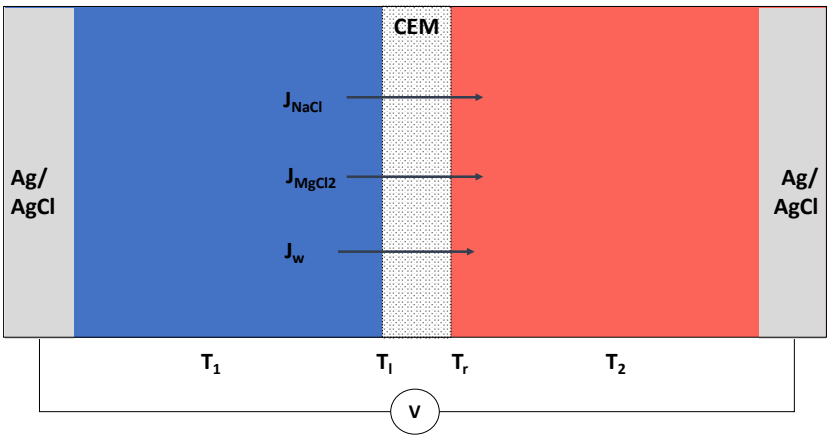

Figure 4.1: Model of the thermocell, with notation used in the equations.

Where $J_q^{\prime(r)}$ is the measurable heat flux at side r of the surface, MCl_z is either NaCl or MgCl_2, and J_{MCl_z} is the net flux of the salt from compartment 1 to compartment 2. The electric current density is

$$j = L_{\phi q}\Delta_m\left(\frac{1}{T}\right) - L_{\phi w}\frac{\Delta_m\mu_w(T_l)}{T_l} - \sum_{\mathrm{MCl}_z} L_{\phi\mathrm{MCl}_z}\frac{\Delta_m\mu_{\mathrm{MCl}_z}(T_l)}{T_l} - L_{\phi\phi}\frac{\Delta_m\phi}{T_l} \tag{4.2}$$

Where L_{ij} are the Onsager phenomenological coefficients. By setting $j = 0$, we get the open-circuit electromotive potential:

$$\Delta_m\phi = -\frac{L_{\phi q}}{L_{\phi\phi}T_r}\Delta_m T - \frac{L_{\phi w}}{L_{\phi\phi}}\Delta_m\mu_w(T_l) - \sum_{\mathrm{MCl}_z}\frac{L_{\phi\mathrm{MCl}_z}}{L_{\phi\phi}}\Delta_m\mu_{\mathrm{MCl}_z}(T_l) \tag{4.3}$$

By evaluating the ratio between the mass fluxes and the electric current flux and use the Onsager reciprocal relations, we find that

$$\begin{aligned}\frac{L_{\phi\mathrm{MCl}_z}}{L_{\phi\phi}} &= \left(\frac{J_{\mathrm{MCl}_z}}{j}\right)_{T,\mu} \equiv \frac{t_{\mathrm{M}^{z+}}}{z_{\mathrm{M}^{z+}}F} \\ \frac{L_{\phi w}}{L_{\phi\phi}} &= \left(\frac{J_w}{j}\right)_{T,\mu} \equiv \frac{t_w}{F}\end{aligned} \tag{4.4}$$

Where we use that when the electrodes are reversible to the chloride ion, $t_{\mathrm{M}^{z+}}/z_+ = t_{\mathrm{MCl}_z}$. The Peltier heat is the heat transported at constant temperature per faraday, and is defined as

$$\Pi \equiv \frac{1}{F}\left(\frac{J_q^{\prime(r)}}{j/F}\right)_T = \frac{L_{\phi q}}{L_{\phi\phi}} \tag{4.5}$$

The electric current through the membrane can be expressed in terms of the ion transport numbers, which is the fraction of the current that is carried by the specific ion. The contribution to the heat is both from the partial molar entropy of the components moving

through the membrane, and from the entropy transported by the ions. In accordance with [2,17], the Peltier heat divided by the temperature on the right-hand side then gives

$$\frac{\Pi}{T_r} = \frac{1}{F}\left[\sum_{\mathrm{M}^{z+}} \frac{t_{\mathrm{M}^{z+}}}{z_{\mathrm{M}^{z+}}}(S^{*(r)}_{\mathrm{M}^{z+}} - S^{(r)}_{\mathrm{MCl}_z}) - t_- S^{*(r)}_{\mathrm{Cl}^-} - t_w S^{(r)}_w\right] \tag{4.6}$$

Where S_j is the partial molar entropy of component j and S^*_i is the entropy transported reversibly by ion i. The Seebeck effect is an electric potential created by a temperature gradient, and the Seebeck coefficient is the open-circuit cell potential divided by the cell temperature difference. The contribution from the membrane to the Seebeck coefficient of the cell can now be found from (4.3):

$$\eta^m_s \equiv \left(\frac{\Delta_m \phi}{\Delta_m T}\right)_{\Delta\mu(T_l),j=0} = -\frac{L_{\phi q}}{L_{\phi\phi} T_r} = -\frac{\Pi}{T_r} \tag{4.7}$$

Assuming that the transported entropies are constant through the membrane, the position superscript can be dropped. The Seebeck coefficient becomes

$$\eta^m_s = -\frac{1}{F}\left[\sum_{M^{z+}} \frac{t_{\mathrm{M}^{z+}}}{z_{\mathrm{M}^{z+}}}(S^*_{\mathrm{M}^{z+}} - S^{(r)}_{\mathrm{MCl}_z}) - t_{\mathrm{Cl}^-} S^*_{\mathrm{Cl}^-} - t_w S^{(r)}_w\right] \tag{4.8}$$

We will conduct experiments with NaCl and $MgCl_2$. The Seebeck coefficient then takes the form

$$\eta^m_s = -\frac{1}{F}\left[t_{\mathrm{Na}^+}(S^*_{\mathrm{Na}^+} - S^{(r)}_{\mathrm{NaCl}}) + \frac{t_{\mathrm{Mg}^{2+}}}{2}(S^*_{\mathrm{Mg}^{2+}} - S^{(r)}_{\mathrm{MgCl}_2}) - t_- S^*_{\mathrm{Cl}^-} - t_w S^{(r)}_w\right] \tag{4.9}$$

The quantities so far are properties of the membrane. At the solution/ membrane interfaces however, we can assume local equilibrium, and the chemical potentials of the solution and the membrane are equal. At constant temperature, the partial molar entropies can be written as

$$S_{\mathrm{MCl}_z} = S^0_{\mathrm{MCl}_z} - R\ln(m_{\mathrm{M}^{z+}} m^{\nu_-}_{\mathrm{Cl}^-} \gamma^{\nu}_{\pm,\mathrm{MCl}_z}) \tag{4.10}$$

$$S_w = S^0_w - R\ln a_w \tag{4.11}$$

Where m_{Cl^-} is the total chloride concentration of the solution, $\nu = \nu_+ + \nu_-$ are the stoichiometric coefficients of ion dissociation and $\gamma_{\pm,\mathrm{MCl}_z}$ is the mean electrolyte activity. The chemical potential of water, and thus the activity can be evaluated through the Gibbs-Duhem equation:

$$\mathrm{d}\mu_{w,T} = -M_w m_{\mathrm{NaCl}} \mathrm{d}\mu_{\mathrm{NaCl}} - M_w m_{\mathrm{MgCl}_2} \mathrm{d}\mu_{\mathrm{MgCl}_2} \tag{4.12}$$

In terms of activities, this gives

$$\mathrm{d}\ln a_w = -M_w m_{\mathrm{NaCl}} \mathrm{d}\ln(m_{\mathrm{Na}^+} m_{\mathrm{Cl}^-} \gamma^2_{\pm,\mathrm{NaCl}}) - M_w m_{\mathrm{MgCl}_2} \mathrm{d}\ln(m_{\mathrm{Mg}^{2+}} m^2_{\mathrm{Cl}^-} \gamma^3_{\pm\mathrm{MgCl}_2}) \tag{4.13}$$

At low concentrations, the water entropy can be approximated by

$$S_w = S_w^0 + RM_w m_{\mathrm{NaCl}} \ln(m_{\mathrm{Na^+}} m_{\mathrm{Cl^-}} \gamma_{\pm,\mathrm{NaCl}}^2) + RM_w m_{\mathrm{MgCl_2}} \ln(m_{\mathrm{Mg^{2+}}} m_{\mathrm{Cl^-}}^2 \gamma_{\pm,\mathrm{MgCl_2}}^3) \quad (4.14)$$

The Seebeck coefficient now becomes

$$\begin{aligned}\eta_s^m = -\frac{1}{F}[&t_{\mathrm{Na^+}}(S_{\mathrm{Na^+}}^* - S_{\mathrm{NaCl}}^\circ + 2R\ln(m_{\mathrm{Na^+}} m_{\mathrm{Cl^-}} \gamma_{\pm,\mathrm{NaCl}}^2)) \\ &+ \frac{t_{\mathrm{Mg^{2+}}}}{2}(S_{\mathrm{Mg^{2+}}}^* - S_{\mathrm{MgCl_2}}^\circ + R\ln(m_{\mathrm{Mg^{2+}}} m_{\mathrm{Cl^-}}^2 \gamma_{\pm,\mathrm{MgCl_2}}^3)) - t_{\mathrm{Cl^-}} S_{\mathrm{Cl^-}}^* \\ &- t_w(S_w^\circ + M_w R(m_{\mathrm{NaCl}} \ln(m_{\mathrm{Na^+}} m_{\mathrm{Cl^-}} \gamma_{\pm,\mathrm{NaCl}}^2) + m_{\mathrm{MgCl_2}} \ln(m_{\mathrm{Mg^{2+}}} m_{\mathrm{Cl^-}}^2 \gamma_{\mathrm{MgCl_2}}^3))] \quad (4.15)\end{aligned}$$

Going back to equation (4.3), the open-circuit potential contribution from the membrane is

$$\Delta_m \phi = \eta_s^m \Delta_m T - \frac{t_w}{F} \Delta_m \mu_w(T_l) - \frac{t_{\mathrm{Mg^{2+}}}}{2} \Delta_m \mu_{\mathrm{MgCl_2}}(T_l) - t_{\mathrm{Na^+}} \Delta_m \mu_{\mathrm{NaCl}}(T_l) \quad (4.16)$$

Where the two last terms are equal to zero when the composition of the solutions are equal.

The solution

Due to possible heat gradients in the solution at the membrane interfaces, the solution can have a contribution to the thermoelectric potential. In the surrounding solutions there is only net transport of ions. The open-circuit potential takes a similar form as in the membrane. Using solutions of identical composition that circulates at both sides of the membrane, concentration polarization is expected to diminish at open-circuit conditions. The contribution to the open-circuit potential is then

$$\Delta_{\mathrm{sol}} \phi = \eta_s^{\mathrm{sol}}(T_l) \Delta_{1,l} T + \eta_s^{\mathrm{sol}}(T_2) \Delta_{r,2} T \quad (4.17)$$

Where the solution contribution η_s^{sol} is similar in form to the contribution to the Seebeck coefficient from the membrane

$$\eta_s^{\mathrm{sol}} = -\frac{1}{F}\left[t_{\mathrm{Na^+}}^{\mathrm{sol}}(S_{\mathrm{Na^+}}^{*,\mathrm{sol}} - S_{\mathrm{NaCl}}) + \frac{t_{\mathrm{Mg^{2+}}}^{\mathrm{sol}}}{2}(S_{\mathrm{Mg^{2+}}}^{*,\mathrm{sol}} - S_{\mathrm{MgCl_2}}) - t_{\mathrm{Cl^-}}^{\mathrm{sol}} S_{\mathrm{Cl^-}}^{*,\mathrm{sol}}\right] \quad (4.18)$$

With the transported entropies and transport numbers being properties of the solution.

The electrodes and the external circuit

Next, we consider the entropy production at the electrodes. At the electrodes we have the reaction

$$\mathrm{Ag_{(s)}} + \mathrm{Cl^-} \rightleftharpoons \mathrm{AgCl_{(s)}} + e^- \quad (4.19)$$

The contribution to the thermoelectric potential from the electrodes is independent of the composition of the solution. The same is true for the external circuit. The thermoelectric potential of the electrodes is [17]

$$\eta_s^{\mathrm{el}} = \frac{1}{F}(S_{\mathrm{Ag}} - S_{\mathrm{AgCl}}) \quad (4.20)$$

The Seebeck coefficient of the external circuit is [17]

$$\eta_s^{\text{ext}} = -\frac{S^*_{\text{e}^-}}{F} \tag{4.21}$$

Temperature dependence of the Seebeck coefficient

Two different methods of measuring the thermoelectric potential has been used. In one, the temperature is kept constant on one side, in the other, the mean cell temperature is kept constant. This motivates an investigation into the temperature dependence of the Seebeck coefficient. The temperature dependence can be expressed through the partial molar heat capacity

$$S_i = S_i(T_0) + c_{p,i}\ln\frac{T}{T_0} \tag{4.22}$$

The temperature dependence of the transported entropies can similarly be defined by the Thomson coefficients of the components:

$$S_i^* = S_i^*(T_0) + \tau_i\ln\frac{T}{T_0} \tag{4.23}$$

The Seebeck coefficient at $T_0 = T_r$ is, as we have previously shown,

$$\eta_s^m(T_r) = -\frac{1}{F}\left[\sum_{\text{M}^{z+}}\frac{t_{\text{M}^{z+}}}{z_{\text{M}^{z+}}}\left(S^*_{\text{M}^{z+}}(T_r) - S_{\text{MCl}_z}(T_r)\right) - t_{\text{Cl}^-}S^*_{\text{Cl}^-} - t_w S_w(T_r)\right] \tag{4.24}$$

However, if we consider the limit of an infinte series of ion exchange membranes between two compartments at $T = T_0$ and $T = T_1$ respectively, each membrane will experience a potential

$$\text{d}\phi = -\frac{1}{F}\left[\eta_s^m(T_r) + \left(\sum_{\text{M}^{z+}}\frac{t_{M^{z+}}}{z_{\text{M}^{z+}}}(\tau_{\text{M}^{z+}} - c_{p,\text{MCl}_z}) - t_{\text{Cl}^-}\tau_{\text{Cl}^-} - t_w c_{p,w}\right)\ln\frac{T}{T_r}\right]\text{d}T \tag{4.25}$$

The sum of these contributions must equal the thermoelectric potential in one membrane between the compartments at $T = T_1$ ans $T = T_0$. When the temperature difference across the membrane is large, the temperature dependence of the entropies must be taken into account. The thermoelectric potential across the membrane is then given by

$$\begin{aligned}\Delta_m\phi &= \eta_s^m(T_r)\Delta T + \int_{T_r}^{T_l}\frac{1}{F}\left(\sum_{\text{M}^{z+}}\frac{t_{M^{z+}}}{z_{\text{M}^{z+}}}(\tau_{\text{M}^{z+}} - c_{p,\text{MCl}_z}) - t_{\text{Cl}^-}\tau_{\text{Cl}^-} - t_w c_{p,w}\right)\ln\frac{T}{T_0}\text{d}T \\ &= \eta_s^m(T_r)\Delta T - \frac{1}{F}\left(\sum_{\text{M}^{z+}}\frac{t_{M^{z+}}}{z_{\text{M}^{z+}}}(\tau_{\text{M}^{z+}} - c_{p,\text{MCl}_z}) - t_{\text{Cl}^-}\tau_{\text{Cl}^-} - t_w c_{p,w}\right)\left[T_l(\ln\left(\frac{T_l}{T_r}\right) - 1) + T_r\right] \\ &= \eta_s^m(T_0)\Delta T + \tau^{\text{obs}} f(T_r, \Delta_{l,r}T)\end{aligned} \tag{4.26}$$

Where $f(T_r, \Delta_{l,r}T)$ can be written as

$$f(T_r, \Delta_{l,r}T) = (T_r - \Delta_{l,r}T)\ln\left(\frac{T_r - \Delta_{l,r}T}{T_r}\right) + \Delta_{l,r}T \tag{4.27}$$

and τ^{obs} is the observed change in the thermoelectric potential with the temperature.

The full thermoelectric potential

We will conduct experiments with identical solutions at both sides of the membrane. We neglect Soret diffusion at the timescale the experiments are conducted, so the only contribution to the electromotive force is the Seeebeck effect. We combine the temperature-dependent contriubution from the membrane, the solutions, electrodes and the external circuit, and get that

$$\Delta\phi = \eta_s^m(T_r)\Delta_{l,r}T + \eta_s^{\text{sol}}(T_l)\Delta_{1,l}T + \eta_s^{\text{sol}}(T_2)\Delta_{r,2}T + (\eta_s^{\text{el}} + \eta_s^{\text{ext}})\Delta_{1,2}T + \tau^{\text{obs}} f(T_r, \Delta_{l,r}T) \tag{4.28}$$

The experiments will be conducted with a constant temperature on the left-hand side at 298 K, and the temperature on the right-hand side will be varied such that the temperature difference of the cell is up to ±15 K. The Seebeck coefficients will therefore be evaluated at 298 K. Variation in the Seebeck effect will, if significant, be evident as a non-linear relation between the electromotive potential and the temperature difference in the experimental data, expressed through τ^{obs}. In the absence of temperature polarization, the contribution from the solution diminish. The transported entropy of electrons in the external circuit is assumed to be small, and will be neglected. Neglecting temperature polarization in the solution, the thermoelectric potential is

$$\Delta\phi = (\eta_s^m + \eta_s^{\text{el}})\Delta_{1,2}T + \tau^{\text{obs}} f(T_2, \Delta_{1,2}T) \tag{4.29}$$

4.1.2 Thermoelectric potential in single-salt solutions

The equations for the thermoelectric potential in single-salt solutions are similar to the ones valid for mixtures. However, in the single-salt experiments conducted with K^+, Mg^{2+} and Ca^{2+}, as well as in the novel membrane experiments, the mean temperature of the thermocell was held constant, in contrast to the measurements of the mixtures, where one compartment was held at a constant temperature, with the consequence that the average temperature varied.

The membrane

For a thermocell at constant mean temperature, it can be shown that [2] to a linear order in temperature, the Seebeck coefficient at constant mean temperarture, $\bar{T}$ is equal to

$$\eta_s^m(\bar{T}) = -\frac{1}{F}\left[\frac{t_{\text{M}^{z+}}}{z_{\text{M}^{z+}}}(S^*_{\text{M}^{z+}} - S_{\text{MCl}_z}(\bar{T})) - t_{\text{Cl}^-}S^*_{\text{Cl}^-} - t_w S_w(\bar{T})\right] \tag{4.30}$$

The solution

With a similar approximation, the solution's contribution to the Seebeck coefficient is

$$\eta_s^{\text{sol}}(T_l)\Delta_{1,l}T + \eta_s^{\text{sol}}(T_2)\Delta_{r,2}T \approx \eta_s^{\text{sol}}(\bar{T})(\Delta_{1,2}T - \Delta_{l,r}T) \tag{4.31}$$

Where

$$\eta_s^{\text{sol}}(\bar{T}) = -\frac{1}{F}\left[\frac{t^{\text{sol}}_{\text{M}^{z+}}}{z_+}(S^{*,\text{sol}}_{\text{M}^{z+}} - S_{\text{MCl}_z}) - t^{\text{sol}}_{\text{Cl}^-}S^{*,\text{sol}}_{\text{Cl}^-}\right] \tag{4.32}$$

The full thermoelectric potential

The contribution to the Seebeck coefficient from the electrodes and external circuit is invariant of the electrolyte, so the thermoelectric potential becomes

$$\Delta\phi = \eta_s^m(\bar{T})\Delta_{l,r}T + \eta_s^{\text{sol}}(\bar{T})(\Delta_{1,2}T - \Delta_{l,r}T) + (\eta_s^{\text{el}} + \eta_s^{\text{ext}})\Delta_{1,2}T \tag{4.33}$$

4.1.3 Single-salt solutions - data reduction

To take temperature polarization into account, it is necessary with estimates of the temperature gradients in the solution. This was obtained by the fluid mechanics simulation in this thesis, where c is defined as the fraction of the temperature difference bulk solutions that is across the membrane. We have that $\Delta_{l,r}T = c\Delta_{1,2}T$, and can rewrite equation (4.33) as

$$\left(\frac{\Delta\phi}{\Delta_{1,2}T}\right) = c\eta_s^m + (1-c)\eta_s^{\text{sol}} + \eta_s^{\text{el}} \tag{4.34}$$

The corrected contriubution from the membrane to the Seebeck coefficient can now be obtained, given that the solution's contribution to the Seebeck coefficient is known. Proceeding with equation 4.30, we include the electrolyte activities similar to the procedure for the mixed electrolyte:

$$\eta_s^m = -\frac{1}{F}\left[\frac{t_{\text{M}^{z+}}}{z_{\text{M}^{z+}}}(S^*_{\text{M}^{z+}} - S^\circ_{\text{MCl}_z} + \nu R\ln(a_{\pm,\text{MCl}_z})) - t_{\text{Cl}^-}S^*_{\text{Cl}^-} - t_w(S^\circ_w - \nu m_{\text{MCl}_z}M_w R\ln(a_{\pm,\text{MCl}_z}))\right] \tag{4.35}$$

Where the water and the electrolyte activities are related through the Gibbs-Duhem equation. Assuming that the transported entropies and transport numbers are constant with the concentration, the Seebeck coefficient is linear with the logarithm of the electrolyte activity:

$$\frac{\partial\eta_s^m}{\partial\ln(a_{\pm,\text{MCl}_z})} = -\frac{\nu R}{z_{\text{M}^{z+}}F}\left(t_{\text{M}^{z+}} - m_{\text{MCl}_z}M_w z_{\text{M}^{z+}}t_w\right) \tag{4.36}$$

Where $(t_{\text{M}^{z+}} - t_w z_{\text{M}^{z+}} m_{\text{MCl}_z}M_w) = t_{a,\text{MCl}_z}$ is referred to as the apparent transport number.

In an analysis of the thermoelectric potential in different electrolytes, it is practical to work with a quantity independent of the concentration. We therefore scale the thermoelectric potential with Faraday's constant and subtract the electrolyte entropy multiplied with the apparent transport number, and define this quantity as Λ_m:

$$\Lambda_m^{\text{MCl}_z} = F\eta_s^m - \frac{t_{a,\text{M}^{z+}}}{z_{\text{M}^{z+}}}S_{\text{MCl}_z} \tag{4.37}$$

$$= t_w(S^\circ_w - mM_wS^0_{\text{MCl}_z}) - \frac{t_{\text{M}^{z+}}}{z_+}S^*_{\text{M}^{z+}} + t_{\text{Cl}^-}S^*_{\text{Cl}^-} \tag{4.38}$$

An important note to this equation is the distinction between the true and apparent transport number of the cation, as both are used in the equation, hence the term $mM_wS^0_{\text{MCl}_z}$. At low concentrations, however, this term is small and can be neglected.

4.1.4 NaCl−$MgCl_2$ solutions - Data reduction

In the following section, a method to analyze the contributions to the thermoelectric potential in the NaCl−$MgCl_2$ system is presented. The methods seek to analyze the contributions to the potential and to relate measurements in the single-salt systems to this system. We will proceed with equation (4.15). Let's now consider two different cases. In the first, only NaCl is present in the solution, and in the second a small amount of $MgCl_2$ is added, while the concentration of Na^+ remains constant. In the pure NaCl solution, $t_{Na^+} = 1 - t_{Cl^-}$ and the membrane Seebeck coefficient then becomes (scaled with -F)

$$\begin{aligned} -F\eta_s^{m,\text{pure}} = (1-t_{Cl^-})(S^*_{Na^+} - S^\circ_{NaCl} + R\ln(m_{Na^+}m^{\text{pure}}_{Cl^-}\gamma^{\text{pure2}}_{\pm,NaCl})) - t_{Cl^-}S^*_{Cl^-} \\ - t_w(S^\circ_w + M_wRm_{NaCl}\ln(m_{Na^+}m^{\text{pure}}_{Cl^-}\gamma^{\text{pure2}}_{\pm,NaCl})) \end{aligned} \quad (4.39)$$

We add $MgCl_2$ assume the following to hold:

1. The chloride transport number is constant.
2. The transported entropies are constant.

In the mixed solution, $t_{Na^+} = 1 - t_{Cl^-} - t_{Mg^{2+}}$. Using this, the corresponding equation is

$$\begin{aligned} -F\eta_s^{m,\text{mix}} &= (1-t_{Cl^-}-t_{Mg^{2+}})(S^*_{Na^+} - S^\circ_{NaCl} + R\ln(m_{Na^+}m^{\text{mix}}_{Cl^-}\gamma^{\text{mix2}}_{NaCl})) \\ &\quad + \frac{t_{Mg^{2+}}}{2}\left(S^*_{Mg^{2+}} - S^\circ_{MgCl_2} + R\ln(m_{Mg^{2+}}m^2_{Cl^-}\gamma^3_{MgCl_2})\right) - t_{Cl^-}S^*_{Cl^-} \\ &\quad - t_w[S^\circ_w + M_wR(m_{NaCl}\ln(m_{Na^+}m^{\text{mix}}_{Cl^-}\gamma^{\text{mix2}}_{NaCl}) + m_{MgCl_2}\ln(m_{Mg^{2+}}m^2_{Cl^-}\gamma^3_{MgCl_2}))] \end{aligned} \quad (4.40)$$

We now consider the difference between the two Seebeck coefficients under the assumption that the transported entropies and the chloride and water transport numbers are the same for both sets of solutions. In the mixed solution, the concentration of $m_{Mg^{2+}} = \epsilon m_{Na^+}$, where $\epsilon >> 1$. The chloride concentration in the mixed solution is $m_{Cl^-} = m_{Na^+}(1+2\epsilon)$. The difference between the Seebeck coefficient in the mixed and the pure solution, $\Delta\eta_s^m$, is

$$\begin{aligned} -F\Delta\eta_s^m &= -F(\eta_s^{m,\text{mix}} - \eta_s^{m,\text{pure}}) \\ &= (1-t_{Cl^-})R\ln\left((1+2\epsilon)\left(\frac{\gamma^{\text{mix}}_{\pm,NaCl}}{\gamma^{\text{pure}}_{\pm,NaCl}}\right)^2\right) + t_{Mg^{2+}}R\ln\left(\frac{(\epsilon m^{\frac{1}{2}}_{Na^+}\gamma^{\frac{3}{2}}_{\pm,MgCl_2}}{m_{Na^+}\gamma^{\text{mix2}}_{\pm,NaCl}}\right) \\ &\quad + t_{Mg^{2+}}\left(\frac{1}{2}(S^*_{Mg^{2+}} - S^0_{MgCl_2}) + S^0_{NaCl} - S^*_{Na^+}\right) - \Delta(t_wS_w) \end{aligned} \quad (4.41)$$

As we expect the water transport number to change with the composition of ions, we may propose a model for the water transport in terms of the ion transport numbers. A simple

model is to assume that the water tranpsort number is proportional to the ion transport numbers, justified by the assumption that electro-osmosis is governing the water transfer:

$$t_w = t_w^{0,\mathrm{Na^+}} t_{\mathrm{Na^+}} + t_w^{0,\mathrm{Mg^{2+}}} t_{\mathrm{Mg^{2+}}} + t_w^{0,\mathrm{Cl^-}} t_{\mathrm{Cl^-}} \tag{4.42}$$

Where $t_w^{0,\mathrm{M}^{z+}}$ would be the water transport number if only ion M^{z+} were transported through the membrane. Studies has shown that systems of divalent and monovalent ions deviate from this model [44], but it provides a usefull relation here. The change in the water transport number is then

$$\Delta t_w = t_{\mathrm{Mg^{2+}}}(t_w^{0,\mathrm{Mg^{2+}}} - t_w^{0,\mathrm{Na^+}}) \tag{4.43}$$

We evaluate the term $\Delta(t_w S_w)$:

$$\begin{aligned}
\Delta(t_w S_w) &= t_w S_w|_{\mathrm{mix}} - t_w S_w|_{\mathrm{pure}} \\
&= t_w^{\mathrm{mix}} \Delta S_w + S_w^{\mathrm{pure}} \Delta t_w \\
&= t_{\mathrm{Mg^{2+}}}(t_w^{0,\mathrm{Mg^{2+}}} - t_w^{0,\mathrm{Na^+}})(S_w^\circ + M_w R m_{\mathrm{Na^+}} \ln(m_{\mathrm{Na^+}}^2 \gamma_{\pm,\mathrm{NaCl}}^{\mathrm{pure2}})) \\
&+ t_w^{\mathrm{mix}} M_w R m_{\mathrm{NaCl}} \left[\ln\left((1+2\epsilon) \left(\frac{\gamma_{\pm,\mathrm{NaCl}}^{\mathrm{mix}}}{\gamma_{\pm,\mathrm{NaCl}}^{\mathrm{pure}}} \right)^2 \right) + \epsilon \ln\left(\epsilon m_{\mathrm{Na^+}}^3 (1+2\epsilon)^2 \gamma_{\pm,\mathrm{MgCl_2}}^3 \right) \right]
\end{aligned} \tag{4.44}$$

Based on measurements by Trivijitkasem and Østvold [45], we can expect the water transport number to be in the range of 5-10 in monovalent cation solutions, and increasing to approximately 20 for divalent cations. The factor $M_w R m_{\mathrm{Na^+}}$ will be smaller than 0.002, and, if we use an upper limit of 20 for the water transport number, the contribution to the potential of $t_w^{\mathrm{mix}} \Delta S_w$ is less than 0.1 μV/K for all concentrations considered here. This justifies the approximation

$$\Delta(S_w t_w) \approx t_{\mathrm{Mg^{2+}}}(t_w^{0,\mathrm{Mg^{2+}}} - t_w^{0,\mathrm{Na^+}}) S_w^\circ \tag{4.45}$$

We insert into (4.41) and get:

$$\begin{aligned}
-F\Delta\eta_s^m &= -F(\eta_s^{m,\mathrm{mix}} - \eta_s^{m,\mathrm{pure}}) \\
&= (1 - t_{\mathrm{Cl^-}}) R \ln\left((1+2\epsilon) \left(\frac{\gamma_{\pm,\mathrm{NaCl}}^{\mathrm{mix}}}{\gamma_{\pm,\mathrm{NaCl}}^{\mathrm{pure}}} \right)^2 \right) + t_{\mathrm{Mg^{2+}}} R \ln\left(\frac{\epsilon^{\frac{1}{2}} \gamma_{\pm,\mathrm{MgCl_2}}^{\frac{3}{2}}}{m_{\mathrm{Na^+}}^{\frac{1}{2}} \gamma_{\pm,\mathrm{NaCl}}^{\mathrm{2mix}}} \right) \\
&+ t_{\mathrm{Mg^{2+}}} \left(\frac{1}{2}(S_{\mathrm{Mg^{2+}}}^* - S_{\mathrm{MgCl_2}}^0) + S_{\mathrm{NaCl}}^0 - S_{\mathrm{Na^+}}^* - (t_w^{0,\mathrm{Mg^{2+}}} - t_w^{0,\mathrm{Na^+}}) S_w^\circ \right)
\end{aligned} \tag{4.46}$$

$t_{\mathrm{Mg^{2+}}}$ from the slope of the change in the Seebeck coefficient.

The first term in equation (4.46) is small. For $\epsilon = 0.03$, the maximum contribution to the thermoelectric potential from this term is 4 μV. Now, if transported entropies and $t_{\mathrm{Mg^{2+}}}$ are independent of the concentration while the ratio $\epsilon = m_{\mathrm{Mg^{2+}}}/m_{\mathrm{Na^+}}$ is held constant, $t_{\mathrm{Mg^{2+}}}$ can be found from (4.46):

$$\left(\partial \Delta\eta_s^m / \partial \ln\left(\frac{\epsilon^{\frac{1}{2}} \gamma_{\pm,\mathrm{MgCl_2}}^{\frac{3}{2}}}{m_{\mathrm{Na^+}}^{\frac{1}{2}} \gamma_{\pm,\mathrm{NaCl}}^{\mathrm{mix2}}} \right) \right)_{\epsilon\ \mathrm{const.}} = -\frac{t_{\mathrm{Mg^{2+}}} R}{F} \tag{4.47}$$

Knowing $t_{\mathrm{Mg^{2+}}}$, the combined contributions from the water transport and the transported entropies can be evaluated.

Relating the change in the Seebeck coefficient to Λ_m.
The gradient of the change in the thermoelectric potential is a quantity that may be experimentally challenging to determine precisely. An alternative approach could be to estimate the magnesium transport number from knowledge about the contributions from the transported entropies and water transport in single-salt solutions. This will rely on the assumption that the transported entropy of Mg^{2+} remains unchanged in the single- and mixed-salt systems. The transported entropies and water transport in single-salt solutions are expressed through $\Lambda_m^{\mathrm{MCl}_z}$,

$$\Lambda_m^{\mathrm{MCl}_z} = F\eta_s^{m,\mathrm{pure}} - t_{a,\mathrm{M}^{z+}} S_{\mathrm{MCl}_z} \tag{4.48}$$

$$= t_w(S_w^\circ + mM_w S^0_{\mathrm{MCl}_z}) - \frac{t_{\mathrm{M}^{z+}}}{z_+} S^*_{\mathrm{M}^{z+}} + t_{\mathrm{Cl}^-} S^*_{\mathrm{Cl}^-} \tag{4.49}$$

The term $mM_w S^0_{\mathrm{MCl}_z}$ is small and can be neglected. $t_{\mathrm{M}^{z+}}$ is close to unity for selective membranes in dilute, single-salt solutions. Within these approximations, we have the following Λ_m's For Na^+ and Mg^{2+}:

$$\Lambda_m^{\mathrm{NaCl}} \approx t_w^{0,\mathrm{Na}^+} S_w^\circ - S^*_{\mathrm{Na}^+} \tag{4.50}$$

$$\Lambda_m^{\mathrm{MgCl_2}} \approx t_w^{0,\mathrm{Mg}^{2+}} S_w^\circ - \frac{1}{2} S^*_{\mathrm{Mg}^{2+}} \tag{4.51}$$

Where we have introduced the same notation for the water transport numbers as in equation (4.42). Inserting into (4.46) and neglecting the first term yields

$$-F\Delta\eta_s^m = t_{\mathrm{Mg^{2+}}} R\ln\left(\frac{\epsilon^{\frac{1}{2}}\gamma_{\pm,\mathrm{MgCl_2}}^{\frac{3}{2}}}{m_{\mathrm{Na}^+}^{\frac{1}{2}}\gamma_{\mathrm{NaCl}}^{\mathrm{mix2}}}\right) + t_{\mathrm{Mg^{2+}}}\left(S^0_{\mathrm{NaCl}} - \frac{1}{2}S^0_{\mathrm{MgCl_2}} - \Lambda_m^{\mathrm{MgCl_2}} + \Lambda_m^{\mathrm{NaCl}}\right) \tag{4.52}$$

The only unknown here is $t_{\mathrm{Mg^{2+}}}$. If the transported entropies are the same as for systems in single-salt solutions, the method of the slope should yield the same transport number.

4.2 Experimental

The thermoelectric potential in ion-exchange membranes has been measured using a range of different solutions and two different membrane types. The work is divided in three: measurements of the thermoelectric potential in Fumasep FKS 75-μm membranes in single-salt solutions of various chloride salts; measurements of the thermoelectric potential in Fumasep FKS 75-μm membranes in binary NaCl-$MgCl_2$ solutions; and measurements in novel cellulose-derived membranes using NaCl solutions.

4.2.1 experimental setup

A schematic representation of the experimental setup is shown in figure 4.2. Two compartments in which the electrolyte solution flowed, were separated by a stack of membranes. Each of the compartments was connected to a thermostatted water bath (Grant Ecocool LT100 and Grant R2), which circulated the solutions. The volumes of these baths were 5 L. The temperatures in the baths were varied to create a temperature gradient across the membrane. The solutions circulated in the two compartments were otherwise identical. To inhibit large pressure gradients between the compartments, the solutions were allowed to flow from the compartments to the baths via a tube not directly connected to the circulating pump.

A K-type thermocouple and a Ag/AgCl electrode and was placed in each compartment. These were connected to an Agilent 34970A data acquisition unit, simultaneously registering the temperatures and voltage. Before each measurement, the thermocouples were calibrated in a manually stirred ice/water bath.

4.2.2 Preparation of electrodes

The electrodes were prepared by coating silver plates with a thin layer of silver chloride. When the electrodes were refreshed, the old chloride layer was first removed with concentrated NH_3, before treated with silver polish to remove potential oxide depositions. The silver was activated in HNO_3 before a chloride was deposited by oxidizing the electrodes in a 1M HCl solution, by sending electric currents of about 2.5 mA through the electrodes for several hours. The electrodes were stored dark in 0.01M HCl to inhibit silver chloride decomposition and short-circuited to eliminate bias potential. The electrodes were refreshed when the bias during experiments exceeded a few hundred μV.

4.2.3 Preparation of membranes

Before experiments with each species of ions, the membranes were pretreated by driving an electric current through them, to exchange the ions in the membrane. The electrodes were connected to a power source and electric currents were driven through the membrane

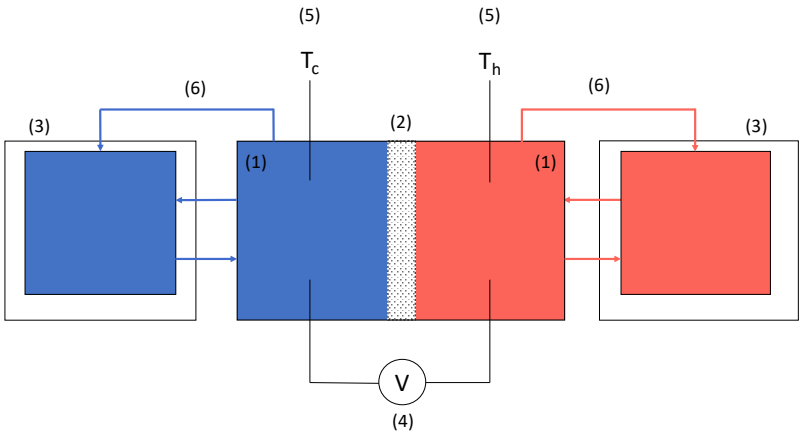

Figure 4.2: schematic representation of the experimental setup used for all experiments in this thesis. The electrolyte flows in two chambers (1) on each side of the stack of ion exchange membranes (2). The solutions are circulated through two thermostatted baths (3), keeping the temperature constant. The cell potential is measured on each side of the membrane stack with two Ag/AgCl electrodes (4). The temperature is measured with K-type thermocouples (5) in the flow-chambers. To inhibit pressure gradients, the solution is allowed to flow through an additional tube (6) between the flow-chamber and the respective bath.

until the total flow of ions had exceeded the membrane ion exchange capacity. At least one week before each experiment, the membranes were immersed in a solution at the same concentration as would be used in the following experiment, and the solutions were changed each second day.

4.2.4 FKS membranes in single-salt solutions

The thermoelectric potential was measured over a stack of 10 FUMASEP FKS-75 μm cation exchange membranes, immersed in single-salt solutions of alkali- and alkaline-earth chlorides. The FKS-75 μm membranes are homogenous, reinforced, with an ion-exchange capacity fo 1-1.25 mmol/g and a thickness of 74-87 μm. Solutions were prepared with deionized water (Merck Millipore) and KCl (Merck pro analysi), $CaCl_2$ (Honeywell Fluca) and $MgCl_2-6\,H_2O$ (Merck pro analysi). The salts were weighed out on a Sartorius balance with 0.001 g accuracy. Measurements were conducted with solutions of 0.3, 0.1, 0.05, 0.01 and 0.001 mol/kg KCl, $CaCl_2$ and $MgCl_2$.

Measurements were conducted at a constant average temperature of 25 °C and the temperatures in the water baths were adjusted to create temperature differences of 20, 10, 0, -10 and -20 °C. The temperature and voltage were measured simultaneously at each temperature difference, when the temperature and voltage were stable.

4.2.5 FKS membranes in NaCl$-$MgCl$_2$ solutions

The thermoelectric potential was measured over a stack of 10 FUMASEP FKS-75 μm cation exchange membranes, immersed in pure NaCl and ternary NaCl$-MgCl_2$ solutions. The measurements were conducted to measure the effect on the thermoelectric potential of adding small amounts of $MgCl_2$ to solutions of NaCl. This was done by measuring the thermoelectric potential in pure NaCl solutions (0.001, 0.005, 0.01 and 0.025 mol/kg) and in solutions with the same concentration of NaCl, but with a small amount of $MgCl_2$, such that the molal concentration ratio $m_{\mathrm{Mg}^{2+}}/m_{\mathrm{Na}^{+}}$, which is referred to as ϵ in the data reduction section, was kept constant for all concentrations. Two series of measurements with NaCl$-MgCl_2$ were conducted, one with $m_{\mathrm{Mg}^{2+}}/m_{\mathrm{Na}^{+}} = 0.02$, and one with $m_{\mathrm{Mg}^{2+}}/m_{\mathrm{Na}^{+}} = 0.03$.

The solutions were prepared from deionized water (Merck Millipore), $MgCl_2-6\,H_2O$ (Merck pro analysi) and NaCl (analaR NORMAPUR), weighed out on a balance of 0.001 g accuracy. For the most dilute concentrations, $MgCl_2$ was weighed out from a 0.05 mol/kg solution to ensure that the error in the concentration of Mg^{2+} not exceeded an order of 1%.

The temperature in one of the baths was kept constant at 25 °C, and the temperature in the other bath was varied such that the temperature difference between the two was 15, 10, 0, -10 and -15 °C. the temperature and voltage were measured simultaneously,

after stable conditions were obtained at each temperature difference. Measurements were recorded at 15-second intervals for approximately 10 minutes.

4.2.6 FKS membranes in seawater

The thermoelectric potential was measured over a stack of 10 FUMASEP FKS-75 μm cation exchange membranes equilibrated in seawater. The seawater sample was obtained from Trondheimfjorden, at Lade. The salinity was determined weighing a sample of seawater, before boiling off the water and weighing the residue. The water was heated to 85 °C before storage to inhibit algae growth. 10 membranes were placed in the seawater solution for 10 days, with the solution being changed every second day. Measurements were conducted following the same procedure as for the NaCl–$MgCl_2$ systems, with one compartment held at a constant constant temperature while varying the temperature in the other compartment.

4.2.7 Cellulose-based membranes

The thermoelectric potential was measured in novel, cellulose-derived membranes provided by PFI. The two membranes will be referred to as membrane E and T, and membrane T has a more crosslinked structure than membrane E. The two membranes were immersed in a 0.1 mol/kg NaCl solution, and the solutions were replaced every second day the first week. Neither membranes showed signs of degradation in the solutions, but the membranes were fragile and prone to fractures. This was, in particular, true for membrane E. Both membranes were without reinforcement material. Due to their fragility, an attempt to pretreat them by driving currents of ions - which has been done for the other membranes in this thesis - was not made. To prevent breakage during measurements of the thermoelectric potential, two reinforcement strategies were employed. One was to use standard laboratory filter paper (VWR, 12-15 μm particle retention size) on each side of the membrane. The other strategy was to use a metal grid on each side of the membrane. The metal grid allowed direct contact between the solution and the membrane. Measurements of membrane E was done in combination with 4 filter papers (two on each side) and metal grids. Measurements of membrane T was done in combination with two and four filter papers and with metal grids. One control measurement was also conducted with only four filter papers. One additional measurement of membrane T in a 0.01 mol/kg NaCl solution, with metal grids as support material, was also conducted. The measurements of the temperature and voltage followed the same procedure as in the single-salt measurements: the mean temperature was kept constant at 25 °C, while the measurements were conducted at temperature differences of 20, 10, 0, -10 and -20 °C. Table 4.1 shows the physical appearance of the membranes

Membrane	Thickness [μm]	Stability
E	19 $\pm$2	Stable in 0.1 mol/kg NaCl. Fragile.
T	22 ± 2	Stable in 0.1 mol/kg.
Filter paper	110	-

Table 4.1: Physical properties and apparence of cellulose-based membranes and thickness of filter (used as support material)

4.3 Results and discussion

The experimental results will be presented in the following sections. First, the results from the measurements in single-salt solutions are presented. Temperature polarization is taken into account in this analysis, so values of the solution's contribution to the Seebeck coefficient obtained from the literature will be presented as well. In the mixed-salt solutions, the analysis follows the methods outlined in 4.1.4. In light of these results and the results from the single-salt solutions, the results from the seawater sample are presented and discussed. Lastly, results from the novel, cellulose-based membranes are presented and discussed.

4.3.1 FKS membranes in Single-salt solutions

The Seebeck effect was measured in solutions of $CaCl_2$, $MgCl_2$ and KCl. The thermoelectric potential at a given electrolyte concentration was calculated from simultaneous measurements of the cell potential and the cell temperature difference. A linear relationship between the temperature difference and the cell potential was observed in all cases. A linear model was applied using least-squares linear regression of the mean voltage and temperature difference at each temperature difference. The thermoelectric potential was taken as the slope of this linear model. Results from pure NaCl solutions will also be included in this section. These were obtained for the purpose of analyzing the NaCl$-$$MgCl_2$ system, but are also relevant for the analysis here.

From the CFD study of the thermocell, we expect temperature polarization to be present. This can be accounted for using equation (4.34), with $c = 0.877$, obtained from the CFD simulations. To find the contribution to the Seebeck coefficient from the solution, values of the solution Seebeck coefficients were obtained from the literature. While this quantity is hardly found directly, it can be calculated from certain experimental data. The solution Seebeck coefficient of KCl solutions was calculated from data reported by Ratkje [46], where the thermoelectric potential was measured in homogenous solutions of KCl, using Ag/AgCl electrodes. The solution Seebeck coefficients of $MgCl_2$ and $CaCl_2$ solutions were calculated from data by Petit et al. [47] who measured the Soret effect in solutions of alkali earth chloride solutions. This was done by measuring the difference between the initial thermoelectric potential and the potential at Soret equilibrium. The

initial thermoelectric potentials in these solutions were measured at uniform composition, and corresponds to the Seebeck coefficient measured here. These experiments were also conducted with Ag/AgCl electrodes. The solution Seebeck coefficients were therefore found by subtracting the electrode contribution from the thermoelectric potential:

$$\eta_s^{\mathrm{sol}} = \left(\frac{\Delta\phi}{\Delta T}\right)_{j=0} - \eta_s^{\mathrm{el}} \tag{4.53}$$

Where η_{el} is calculated from the standard entropies of Ag and AgCl. Using $S^{\circ}_{\mathrm{Ag}} = 42.6$ J/K mol and $S^{\circ}_{\mathrm{Ag}} = 96.3$ J/K mol [48], η_{el} is -0.557 mV/K, invariant of the concentration and electrolyte. η_s^{sol} showed in all cases a linear relationship with the logarithm of the electrolyte activity, this can be seen in figure 4.3. Activity coefficients were calculated with Pitzer's equations [49] (equations and a comparison with literature values are given in appendix B). A linear model was fitted to each set of Seebeck coefficients, and this linear model was used to estimate the Seebeck coefficient for the concentrations used in this thesis.

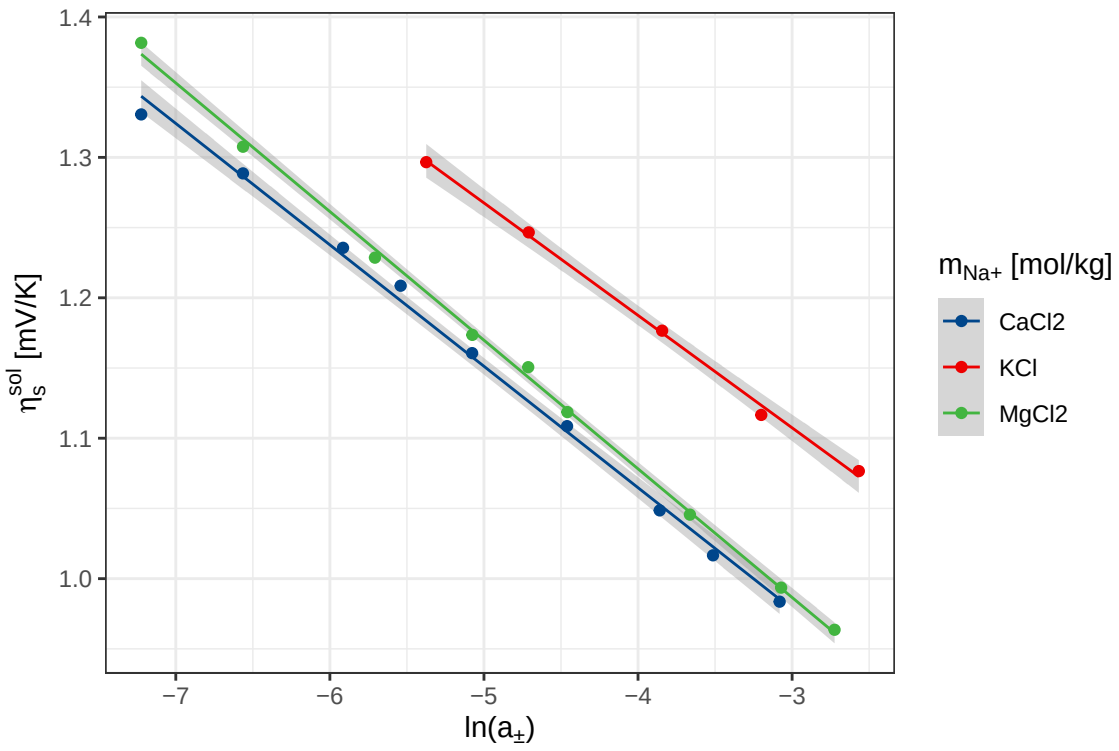

Figure 4.3: Solution Seebeck coefficients obtained from the literature [46, 47],with least-square linear fits. The gray areas indicate 95% confidence intervals.

In the case of NaCl, a similar data series was not found, so the values of the reported thermoelectric potential and sodium tranport number at 0.01 mol/kg [50], was used to calculate $t^{\mathrm{sol}}_{\mathrm{Na}^+} S^*_{\mathrm{Na}^+} - t^{\mathrm{sol}}_{\mathrm{Cl}^-} S^*_{\mathrm{Cl}^-}$, and use this in equation 4.32 with the assumption that the transported entropy and sodium transport number in the solution is constant. Estimated Seebeck coefficients at relevant concentrations are shown in table 4.2.

m[mol/kg]	$\eta^{\text{sol}}_{\text{NaCl}}$ [mV/K]	$\eta^{\text{sol}}_{\text{KCl}}$ [mV/K]	$\eta^{\text{sol}}_{\text{MgCl}_2}$ [mV/K]	$\eta^{\text{sol}}_{\text{CaCl}_2}$ [mV/K]
0.3		0.98	0.302	0.259
0.1	1.04	1.06	0.385	0.349
0.05		1.12	0.437	0.405
0.025	1.13			
0.01	1.20	1.24	0.561	0.538
0.005	1.24			
0.001	1.35	1.43	0.758	0.747

Table 4.2: Electrolyte Seebeck coefficients calculated with emf-data from [46, 47, 50].

The membrane Seebeck coefficient corrected for temperature polarization is presented in figure 4.4, while their exact values are given in table 4.3. Values of the membrane Seebeck coefficient where temperature polarization is neglected are given in Appendix C. The Seebeck coefficient is, in general, higher for the monovalent ions than the divalent ions, and shows in all cases a linear dependence on the electrolyte activity. The linear dependence is expected from equation (4.36). Least-squares linear models were fitted to the membrane Seebeck coefficients vs. the electrolyte activities, and the apparent transport numbers were calculated from the slope of these models. Apparent transport numbers are shown in table 4.4, both with polarization being included and neglected. The effect of including temperature polarization is that the estimate of η_s^m becomes higher than when polarization is neglected, since the solution's contribution to the Seebeck coefficient in all cases is lower than the membrane's. The apparent transport numbers of the monovalent ions also show a small increase when temperature polarization is taken into account. This is expected as the unselective transport in the thermal boundary layers in the solutions in this case is accounted for. The same is not observed for Ca^{2+}, however, where a small increase is observed. The increase is not significant, so it could be due to errors in the estimates. For the apparent transport numbers, the largest deviation between the corrected and uncorrected values are seen for the monovalent ions. However, the estimates are also more uncertain, both due to uncertainties in the estimated temperatures, and due to the errors in η_s^{sol}, as these are linear interpolation and extrapolation estimates.

For Na^+, the apparent transport numbers agree well with the literature. Kristiansen et al. estimated the apparent transport number in 20 FKS membranes from thermoelectric potential measurements, and found $t_{a,\text{Na}} = 0.89 \pm 0.05$, which is similar to the value found here, when temperature polarization is neglected. At isothermal conditions Na^+ in FKS-membranes has been found to have a transport number of 0.93 ± 0.03 [51]. The divalent ions, however, have significantly lower transport numbers. This could be attributed to a higher membrane resistance when using divalent ions [52, 53] leading to a larger co-ion transport.

It's worth noting that the Seebeck coefficients in the systems with and without a sepa-

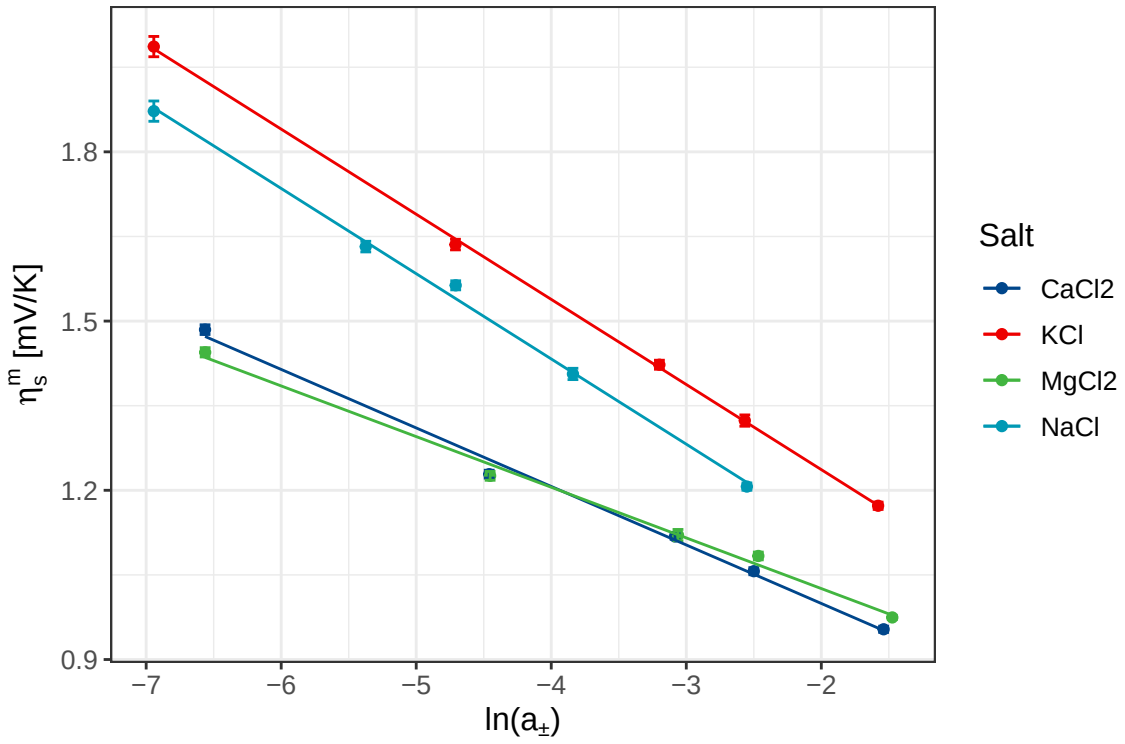

Figure 4.4: Membrane Seebeck coefficients of KCl, $CaCl_2$ and $MgCl_2$ plotted against logarithm of the electrolyte activity.

rating membrane are of the same order of magnitude. This suggests that a substantial potential difference could be created solely by sustaining a temperature gradient between the electrodes, even with unselective membranes. The trends in the Seebeck coefficients with respect to the ions is also similar, with KCl generally having the highest and the divalent ions having the lowest Seebeck coefficients. This indicates that, in a search for ions yielding the highest membrane Seebeck coefficients, an investigation of the ions' solution Seebeck coefficients would be a reasonable starting point.

The thermoelectric potential is dependent on the electrolyte concentration, and in an analysis of the relation between the ion species and the Seebeck coefficient it is useful to investigate a quantity where this concentration dependence is removed. We therefore introduce Λ_m as defined in equation (4.38). Λ_m for the different ions and concentrations are shown in figure 4.5. There is a clear and consistent separation between the ions, with the divalent ions being positive and the monovalent being negative. Average values are shown in table 4.5. This motivates a search for a relation between the Λ_m-values. A correlation with the hydrated radius of the ions measured by Nightingale [54] is evident, and figure 4.6 shows Λ_m plotted against the cube of the hydrated radius. There are too few data points to be conclusive about the nature of the relationship between the quantities. one could, however, propose a relationship between the two quantities by relating volume of the hydration shells of the ions, which is proportional to r_h^3, to the water transport number t_w. Following this reasoning, the difference in the Λ_m-values could be explained

m [mol/kg]	η^{m}_{NaCl} [mV/K]	η^{m}_{KCl} [mV/K]	$\eta^{m}_{MgCl_2}$ [mV/K]	$\eta^{m}_{CaCl_2}$ [mV/K]
0.3		1.200 ± 0.007	0.991 ± 0.004	0.967 ± 0.006
0.1	1.238 ± 0.008	1.36 ± 0.01	1.18 ± 0.008	1.073 ± 0.007
0.05		1.466 ± 0.009	1.22 ± 0.01	1.137 ± 0.006
0.025	1.45 ± 0.01			
0.01	1.63 ± 0.01	1.69 ± 0.01	1.32 ± 0.009	1.246 ± 0.008
0.005	1.69 ± 0.01			
0.001	1.93 ± 0.03	2.06 ± 0.02	1.51 ± 0.009	1.51 ± 0.01

Table 4.3: Membrane seebeck coefficients, corrected for temperature polarization, with equation (4.34)

.

Ion	t_a, temperature polarization incl.	t_a, temperature polarization negl.
K^+	0.93 ± 0.02	0.88 ± 0.02
Na^+	0.92 ± 0.08	0.89 ± 0.05
Mg^{2+}	0.69 ± 0.06	0.69 ± 0.06
Ca^{2+}	0.82 ± 0.07	0.80 ± 0.06

Table 4.4: Apparent membrane transport numbers, calculated from (4.36)

by different water transport numbers. However, given that $S^{\circ}_{w} \approx 70$ J/K mol, and the water transport number of membranes typically are 5-10 in monovalent solutions and up to 20 in divalent solutions [45], we should expect variations in Λ_m in the order of 700 J/K mol, not 100-150 J/K mol. Thus, either the water transport in the FKS membranes used here is considerably lower, or there are variations in the transported entropies that counteract the effect of water transport.

Salt	Λ_m [J/K mol] (polarization incl.)	Λ_m [J/K mol] (polarization negl.)
$CaCl_2$	53 ± 5	53 ± 5
$MgCl_2$	90 ± 2	92 ± 2
KCl	-56 ± 5	-49 ± 4
NaCl	-24 ± 12	-21 ± 8

Table 4.5: Values of Λ_m, with and without temperature polarization being taken into account

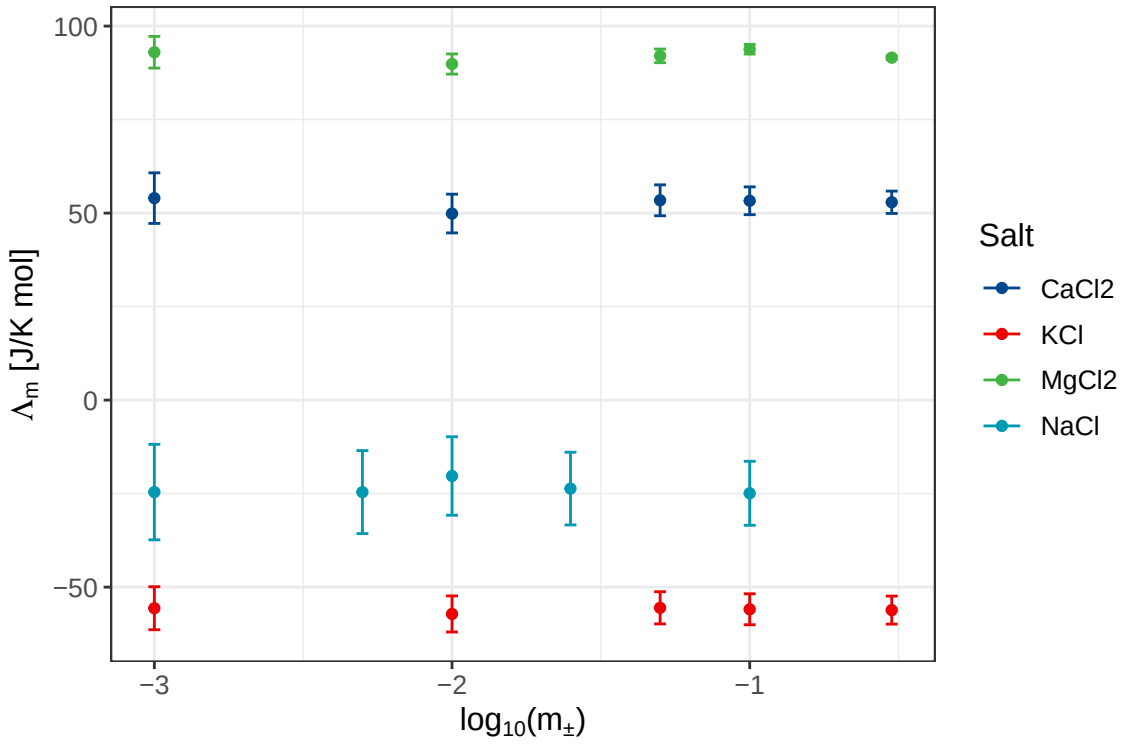

Figure 4.5: Λ_m values of the ions as defined by equation (4.38), corrected for temprature polarization. Error bars indicate double standard deviations.

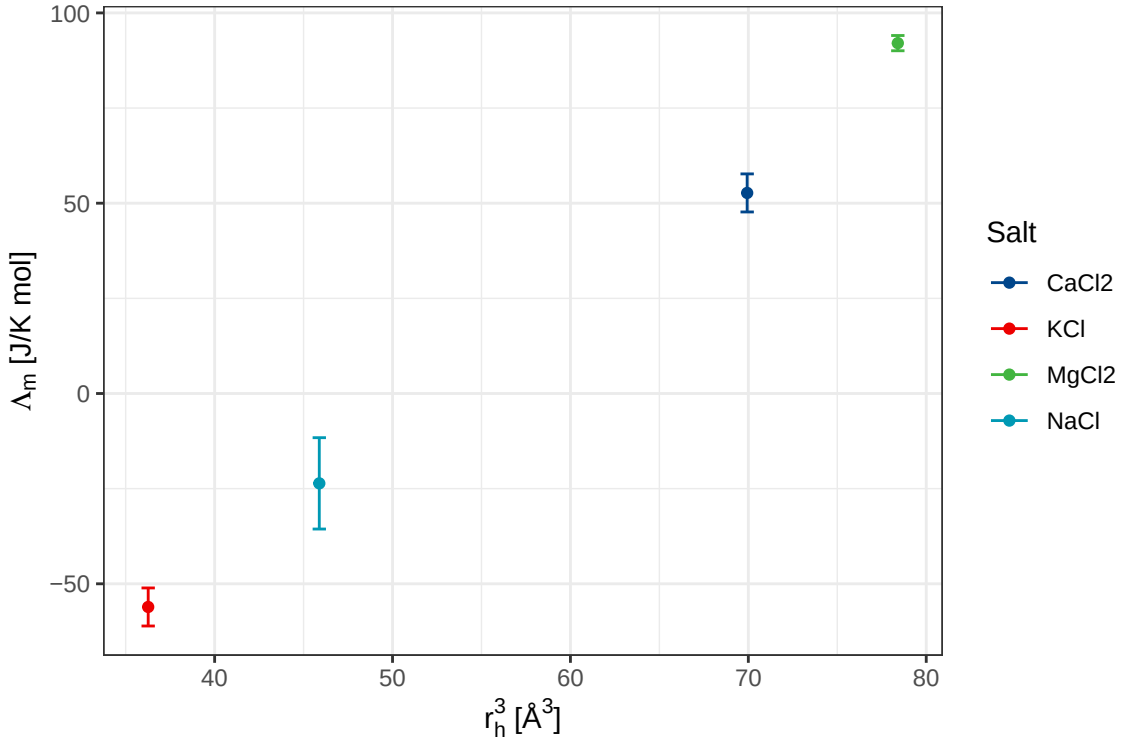

Figure 4.6: Average values of Λ_m plotted against the cube of the ions' hydrated radius. The plot serves to show an apparently linear relationship between the two quantities.

4.3.2 FKS membranes in NaCl−$MgCl_2$ systems

The Seebeck effect was measured in pure NaCl-solutions, and binary solutions of NaCl and $MgCl_2$. For each temperature difference, a series of temperature and cell voltage measurements were obtained. The relation between the cell potential and the temperature had a small, but consistent non-linear component. Hence, a multilinear regression model based on equation (4.29) was fitted to the mean temperature differences and voltages. Figure 4.7 shows a representative measurement of the cell voltage vs. the temperature. Uncertainties were estimated with case bootstrapping of the individual temperature difference and corresponding cell voltage measurements, to capture the variance both between and within each cluster of measurements [55]. That is, pairwise samples of the temperature difference and cell voltage were drawn from each cluster. The regression model was fitted to the samples to obtain bootstrap estimates of the coefficients, and the standard deviation was estimated from the distribution of the bootstrap estimates obtained by repeating this procedure.

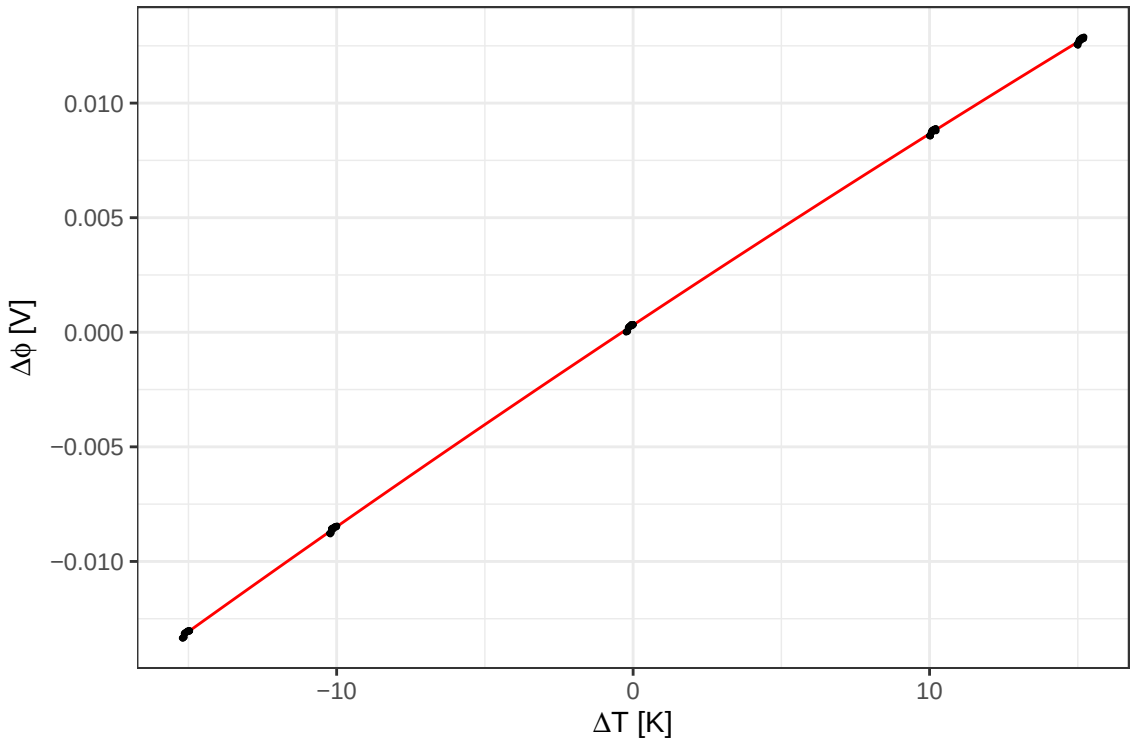

Figure 4.7: Representative plot of cell voltage against the measured temperature difference, with 0.01 mol/kg NaCl and 0.0003 mol/kg $MgCl_2$. At each stable temperature difference, a series of measurements is visualized as a cluster of datapoints. The red line is the curve fitted from the average temperature and cell voltage of each cluster. The line fits the data well, and is slightly curved due to the temperature dependce of the Seebeck coefficient.

From the CFD simulation of the heat transfer in the thermocell, we expect that the solu-

tion contributes to the thermoelectric potential. This is neglected, however, due to lack of knowledge about the thermoelectric potential in mixed solutions of NaCl and $MgCl_2$. Within this approximation, the membrane's contribution to the Seebeck coefficient is found by subtracting the electrode contribution, η_s^{el} from the coefficient of the linear contribution to the thermoelectric potential. As previously, We find $\eta_s^{\text{el}} = -0.557$ mV/K. Activity coefficients are estimated with Pitzer's equations (Given in Appendix B). Figure 4.8 shows the membrane contribution to the Seebeck coefficients obtained with pure NaCl and NaCl$-$$MgCl_2$ solutions. In the pure NaCl solutions, η_s^m decreases linearly with the activity, this was discussed in the section of single-salt solutions. Figure 4.9 shows the membrane Seebeck effect plotted against ϵ (the molal concentration ratio $m_{\text{Mg}^{2+}}/m_{\text{Na}^+}$), visualizing the effect of adding $MgCl_2$. The membrane potential is in all cases significantly lower, compared with the potential in pure NaCl at the same Na^+ concentraion. In the further analyzis, we will work with the difference between the membrane's contribution to the Seebeck coefficient in the pure NaCl solution and in the NaCl$-$$MgCl_2$ solution at same Na^+ concentration. This quantity is denoted as $\Delta\eta_s^m$, in accordance with the equations in section 4.1.4. There is a tendency that $\Delta\eta_s^m$ is largest at lower concentrations, most pronouncly when $\epsilon = 0.03$. This is as expected from equation (4.47). This tendency comes with a large uncertainty, however. Figure 4.10 and 4.11 show $\Delta\eta_s^m$ when $\epsilon = 0.02$ and $\epsilon = 0.03$ respectively, plotted against $\ln(m_{\text{Mg}^{2+}}^{1/2}\gamma_{\pm,\text{MgCl}_2}^{3/2}) - \ln(m_{\text{Na}^+}\gamma_{\pm,\text{NaCl}}^2)$. Using equation (4.47), we find $t_{\text{Mg}^{2+}}$ to be 0.2 $\pm$0.3 when $\epsilon = 0.02$ and 0.8 $\pm$0.5 when $\epsilon = 0.03$ (values given with double standard deviations). These results indicate thus that $t_{\text{Mg}^{2+}}$ is large compared with the fraction of Mg^{2+} in the solution. The implication of this can be investigated with the mobility model of the ion transport numbers [42, 43]:

$$t_i = \frac{z_i x_i u_i}{\sum_j z_j x_j u_j} \tag{4.54}$$

where x_i is the mole fraction and u_i is mobility of the ion in the membrane. Results have shown that Mg^{2+} increases the membrane resistance [6, 7], so we expect Mg^{2+} to have a lower mobility in the membrane than Na^+. Consequentially, this indicates tha the fraction of Mg^{2+} in the membrane is high relative to the fraction in the solution.

We can also find $t_{\text{Mg}^{2+}}$ using equation (4.52), with values of Λ_m obtained in the single-salt experiments. A graphical representation of these results are shown in figures 4.13 and 4.12. Average values of $t_{\text{Mg}^{2+}}$ obtained with this method are 0.5 $\pm$0.4 when $\epsilon = 0.02$ and 0.7 $\pm$0.5 when $\epsilon = 0.03$(errors given as double standard deviations). For $\epsilon = 0.02$, $t_{\text{Mg}^{2+}}$ is higher in this estimate than with the method of the slope, but this can be due to the large uncertainties in both methods. All the estimated transport numbers of Mg^{2+} are given in table 4.6. The two methods show an agreement that $t_{\text{Mg}^{2+}}$ is large compared with the fraction of Mg^{2+} in the external solution. The agreement of the methods implicates also that the transported entropies do not show major variations with respect to the fraction of ions in the membrane. In the method using Λ_m-values, the transported entropies are assumed to be constant, while this is not a requirement for finding $t_{\text{Mg}^{2+}}$ from the slope of $\Delta\eta_s^m$.

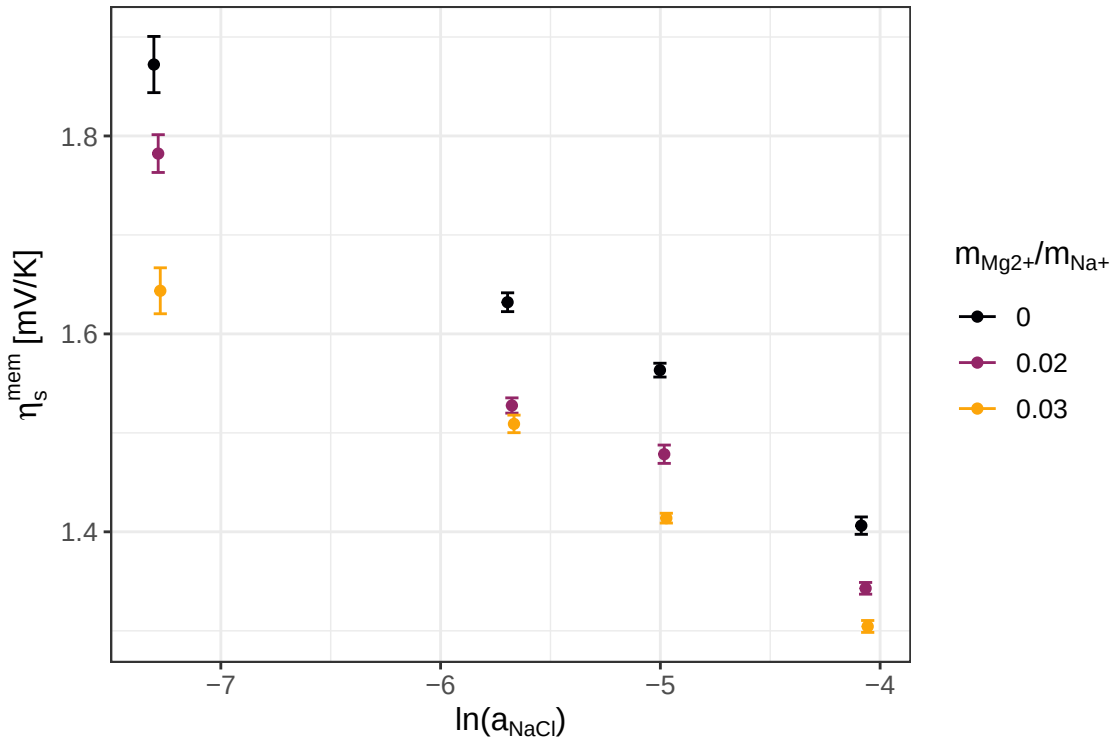

Figure 4.8: Membrane Seebeck coefficients in the NaCl and NaCl−$MgCl_2$ systems, plotted against the activity of NaCl. The error bars indicate the double standard deviation interval of the coefficients.

Method	$\epsilon = 0.02$	$\epsilon = 0.03$
$t_{Mg^{2+}}$ from the slope of η_s^m	0.2 ± 0.3	0.8 ± 0.5
$t_{Mg^{2+}}$ from Λ_m	0.5 ± 0.4	0.7 ± 0.5

Table 4.6: $t_{Mg^{2+}}$ estimated with the two methods outlined in section 4.1.4.

The reasoning behind holding the concentration of Mg^{2+} low relative to the concentration of Na^+ was to keep the properties of the membrane similar to that of the membranes in the pure NaCl solutions. With indications that the concentration of Mg^{2+} in the membrane is much larger than in the external solution, the assumptions made in the data reduction section should be reviewed. t_{Cl^-} and $S^*_{Na^+}$ were assumed to be constant. From the single-salt solutions, the apparent transport number of Mg^{2+} was significantly lower than that of Na^+, however. One could, therefore, expect t_{Cl^-} to increase to a certain degree. The potential errors in these assumptions should have little effect the activity-dependent part of the change in the Seebeck coefficient, thus, the agreement in the two methods for finding $t_{Mg^{2+}}$, suggest that the assumptions made are valid within the accuracy of the experiments.

The results indicate that the transport number of Mg^{2+} is large relative to the concentra-

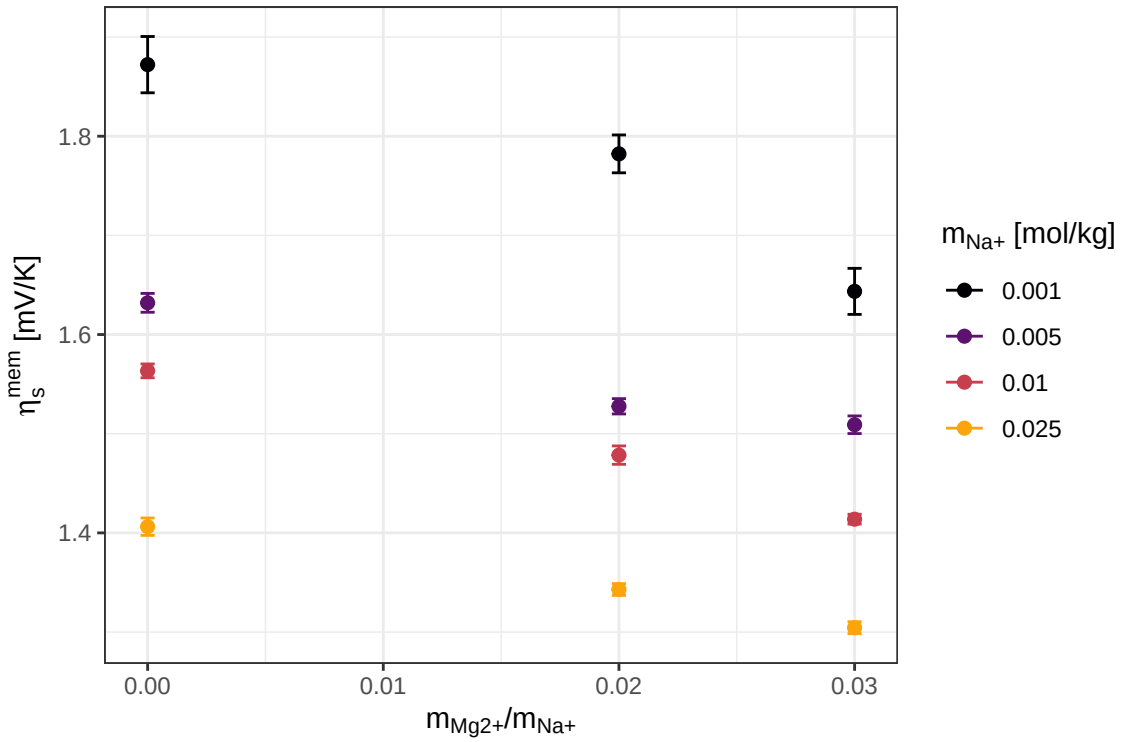

Figure 4.9: Membrane Seebeck coefficients in the NaCl and NaCl-MgCl2 systems plotted against $m_{\mathrm{Mg^{2+}}}/m_{\mathrm{Na^{+}}}$ (ϵ). The error bars indicate the double standard deviation interval of the coefficients.

tion of $MgCl_2$ in the solution, which can be explained by a high concentration of Mg^{2+} ions in the membranes. This has also been observed in conventional RED. Vermaas et al. [7] studied the composition in ion-exchange membranes used in RED with 90 % Nacl - 10 % $MgCl_2$ in the inlet flows, and found that the fraction of Mg^{2+} in the cation exchange membranes were 30 - 60% at steady-state conditions, depending on the membranes used. The higher valence charge of Mg^{2+} leads to a higher affinity for the membrane, and it is thus expected that a large fraction of the current in the membrane is carried by the Mg^{2+} ions. Chapotot et al. [56] studied the competitive transport of Na^{+} and Ca^{2+} in ion exchange membranes, and found that for membranes in equilibrium with the external solution, the concentration of Ca^{2+} in the membrane was much larger than in the solution, due to stronger bonding to the charged groups in the membrane. Their results show that the ratio of the concentration of Ca^{2+} and Na^{+} was up to 45 times higher in the ion-exchange membrane than in the external solution. This was observed both with a conventional CMV-membrane, and with a modified, monovalent-selective membrane.

An important issue when discussing membrane transport numbers in multi-ion systems, is that these may vary with the electric current. It has been predicted [57] that the transport number of Ca^{2+} in $NaCl-CaCl_2$ systems decreases with an increase in the current density. This tendency has been verified experimentally for both Ca^{2+} and Mg^{2+} in desalination of artificial seawater [58]. An explanation for this is that while the affinity

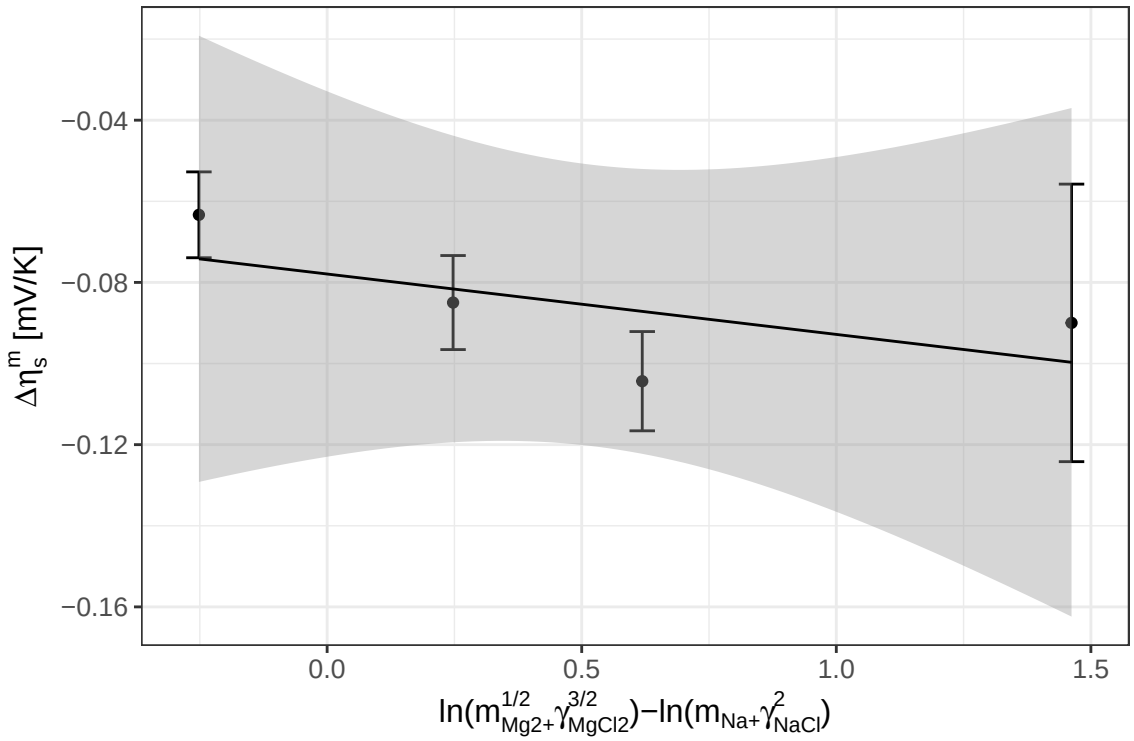

Figure 4.10: Change in the Seebeck coefficient when $\epsilon = 0.02$. The line indicates the least-squares linear fit, and the gray area indicates the 95% confidence interval of the linear fit.

of divalent ions to the membrane is higher, the mobility is lower. There is a transition from when the transport is influenced by the equilibrium composition of the membrane to a transport determined by kinetic properties, to the point that at overlimiting current density conditions, the transport is determined by the ion diffusivity in the concentration boundary layer near the membrane [25]. The experiments in this thesis are conducted with equilibrated membranes at open-circuit conditions, and the transport numbers are governed by the membrane equilibrium composition and the ion mobilities (the mobility model, eq. (4.54)). We cannot, however, expect these transport numbers to be the same in experiments with driving-current conditions.

The composition of ions in the membrane can be described by the equilibrium equation

$$\mathrm{Na{-}X} + \frac{1}{2}\mathrm{Mg}^{2+}_{(\mathrm{aq})} \rightleftharpoons \frac{1}{2}\mathrm{Mg{-}X_2} + \mathrm{Na}^{+}_{(\mathrm{aq})} \tag{4.55}$$

Where X^- is the fixed charge groups in the membrane. Studying a non-isothermal effect, it is relevant to investigate the temperature dependence of this ion-exchange equilibrium. Chaabouni et al. [59] studied the temperature effect of the ion exchange equilibrium between a CMX membrane and binary Na^+-K^+, Na^+-Ca^{2+} and K^+-Ca^{2+} systems, reporting a selectivity order $K^+ > Ca^{2+} > Na^+$, and the selectivity between K^+ and Na^+ was amplified with increasing temperatures from 288 to 313. The opposite was observed for K^+ and Ca^{2+}, where the selectivity towards K^+ decreased with the temperature between 313 and

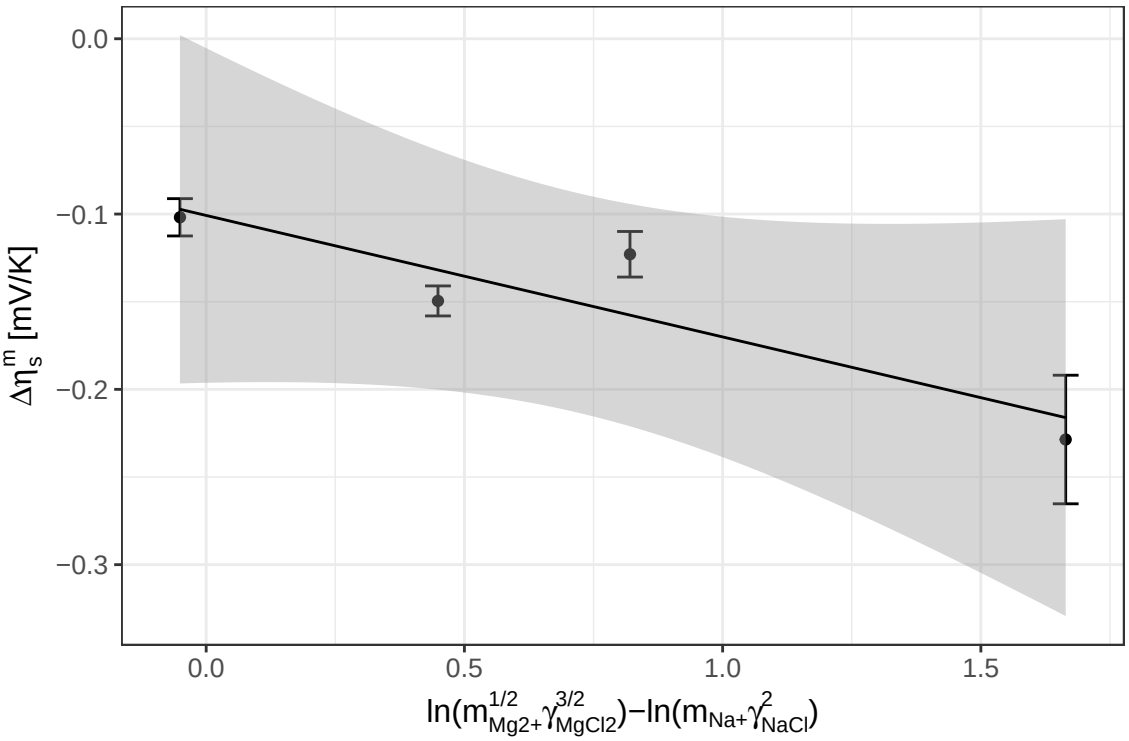

Figure 4.11: Change in the Seebeck coefficient when $\epsilon = 0.03$. The line indicates the least-squares linear fit, and the gray area indicates the 95% confidence interval of the linear fit.

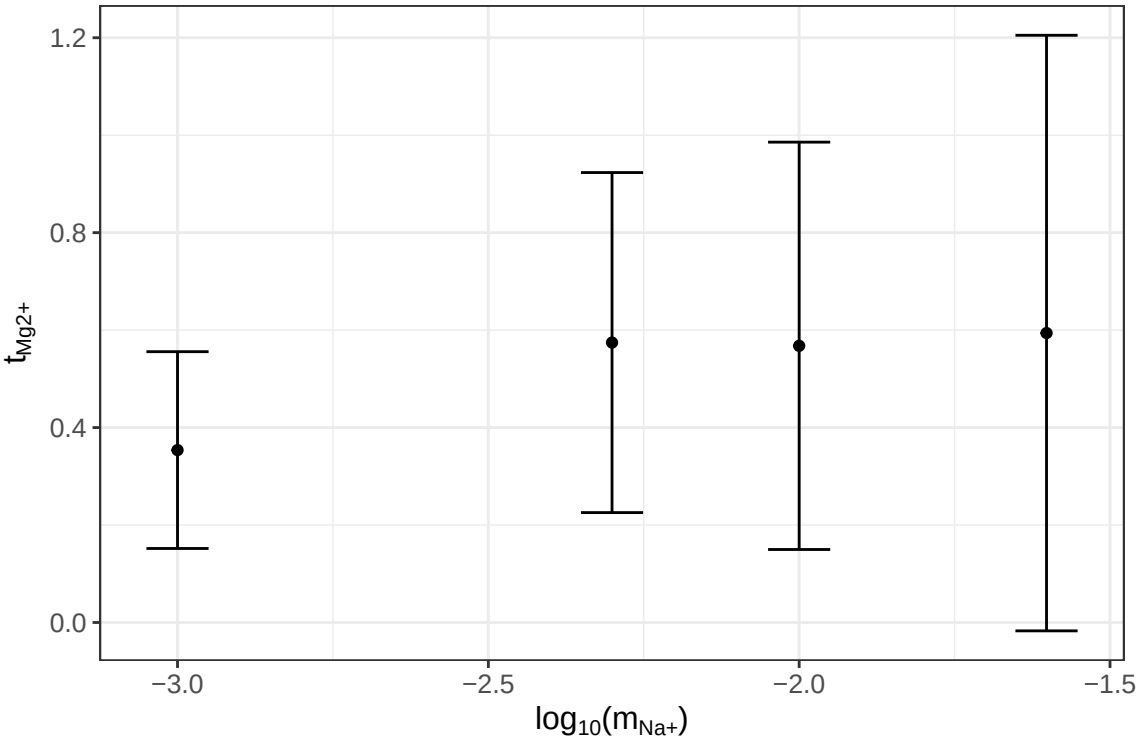

Figure 4.12: Transport numbers calculated from equation REF, when $\epsilon = 0.02$. Error bars indicate double standard deviations.

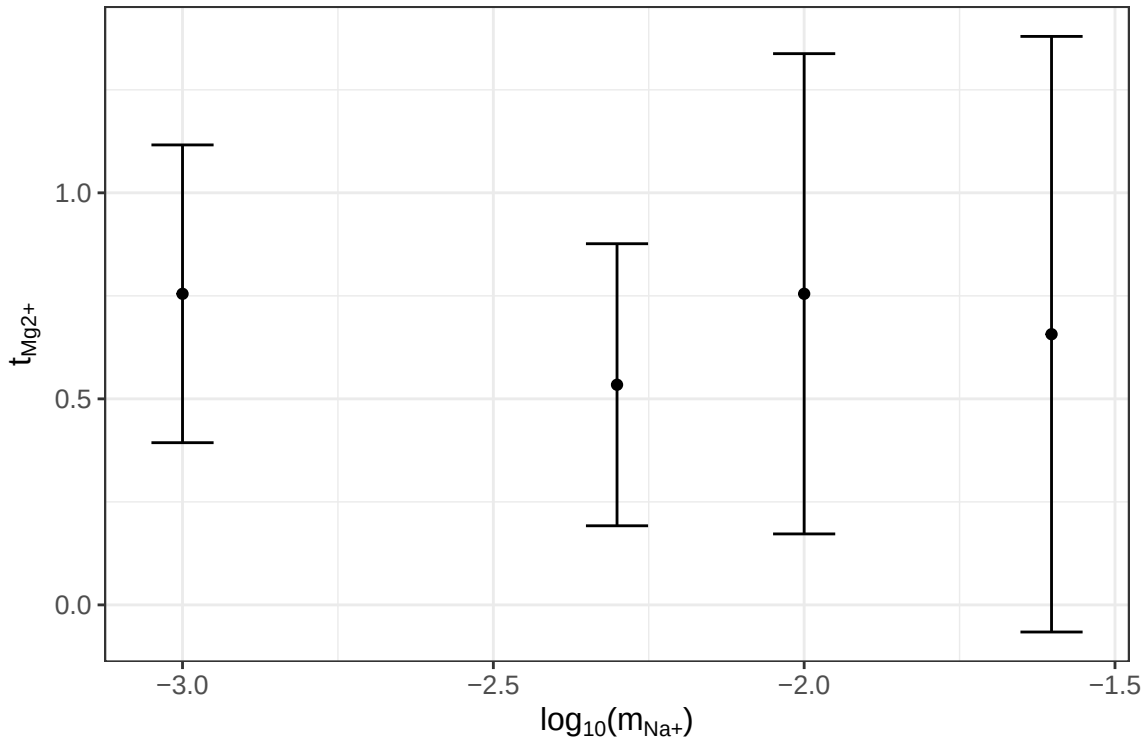

Figure 4.13: Transport numbers calculated from equation REF, when $\epsilon = 0.03$. Error bars indicate double standard deviations.

288 K. We should therefore expect an exchange process to occur between the membrane surface and the solution when the temperature is varied, thus violating the assumption of uniform composition of ions in the membrane. A study on ion-exchange resins in monovalent-divalent solutions by Muraviev et al. [60] showed that the selectivity towards divalent ions increased significantly with the temperature. Moreover, the exchange process occurred on a time-scale of a few minutes. The exchange process was endothermic, explaining the temperature dependence of the selectivity. Based on this we could expect sorption of Mg^{2+} at the hotter membrane surface and desorption at the cold surface. To which degree this occurred and the effect on the measured potentials is unknown, however. But it could explain variations in the measured potentials in the mixed solutions. Benneker et al. [12] studied the effect of temperature gradients in the limiting current regime. An increased temperature in the dilute stream inhibited transport of monovalent ions, while Mg^{2+} was relatively more transported through the membrane, which is inconsistent with what one would expect from the equilibrium properties. This again highlights the importance of the electric current conditions at which experiments are conducted, which must be considered in a process towards pilot testing of thermoelectric-enhanced RED.

A significant temperature dependence of the Seebeck effect (Thomson effect) was observed, and the Thomson coefficients, as defined in equation (4.29) are shown in figure 4.14. The observed Thomson coefficient was negative in all cases, and of the same order of magnitude, between -1 and -3 mV/K. No systematic variation was found with respect

to the fraction of Mg^{2+}, but there is a tendency that the effect is most pronounced at the lowest concentrations. The Thomson coefficients of ion exchange membranes were not found in the literature, but the thermoelectric power has been found to decrease with an increased temperature in liquid junctions with various metal chlorides [46], which agrees with the sign of the observed Thomson coefficient here. The reason that the Thomson effect is present here, and not in the previous single-salt solutions, is because the average cell temperature was held constant in those measurements, leading to a net Thomson effect close to zero.

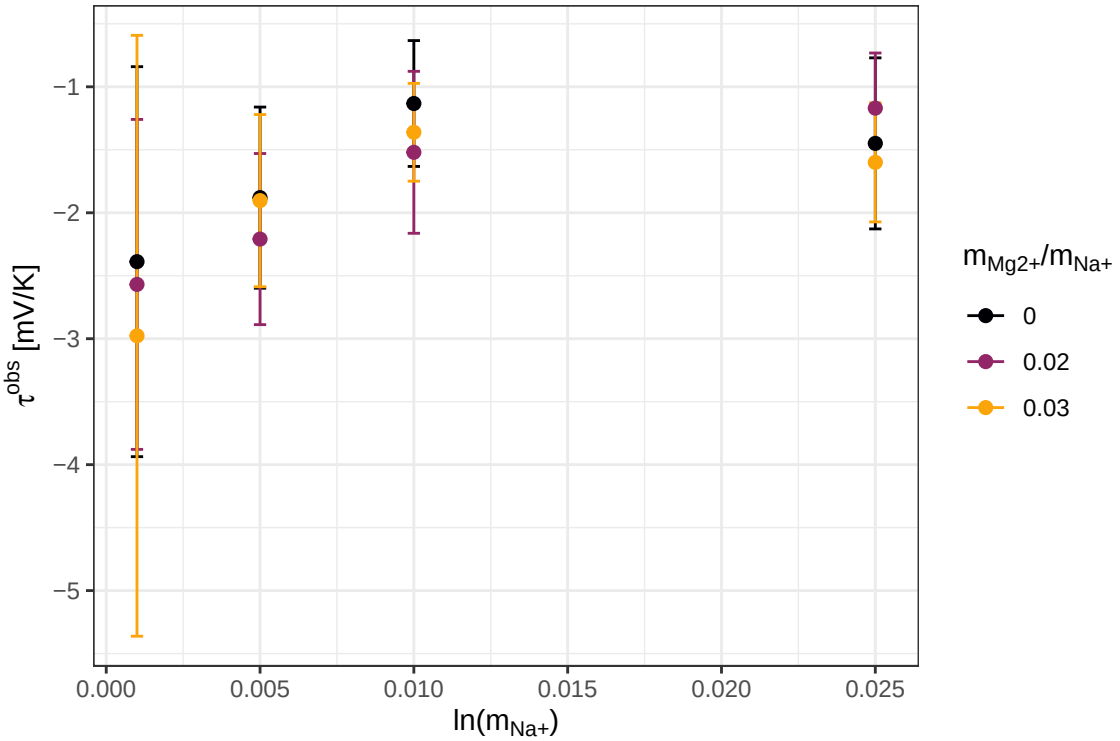

Figure 4.14: Observed Thomson coefficient in the NaCl and NaCl-MgCl2 systems

4.3.3 The thermoelectric potential in seawater

The Sebeebeck effect was measured in a sample of seawater obtained from Trondhjemsfjorden. While the salinity of seawater may show local and seasonal variations, the concentration ratios of the ions are approximately constant [61]. The four most abundant cations in seawater are Na^+, Mg^{2+}, Ca^{2+}, and K^+, and their concentrations were determined from the mass of a seawater sample before and after the water was boiled off, and with concentration data from [62]. The resulting concentrations are shown in table 4.7. It should be noted that the salinity of the sample is almost half that of the ocean average.

The Seebeck coefficient was measured following the procedure of the $NaCl-MgCl_2$ systems. 4.15 shows the plot of the measured thermoelectric potential. The membrane

Ion	m [mol/kg]
Cl^-	0.271
Na^+	0.232
Mg^{2+}	0.026
$SO_4{}^{2-}$	0.014
Ca^{2+}	0.005
K^+	0.005

Table 4.7: Molal concentration of ions in seawater sample

Seebeck effect was found to be 1.216 ±0.004 mV/K with an observed Thomson coefficient of -1.6 ±0.3 mV/K. The Thomson coefficient is in agreement with the coefficient obtained for the more dilute NaCl−$MgCl_2$ solutions, suggesting that the observed Thomson coefficient is showing little variation with the concentration, in the concentration ranges considered here. Using $\Lambda_m^{\mathrm{NaCl}}$ and the apparent transport number of Na^+, we can predict the membrane Seebeck coefficient for a pure NaCl solution at 0.27 mol/kg: $\eta_s^{m,\mathrm{pred}} = \frac{1}{F}(\Lambda_m^{\mathrm{Na}^+} + t_{a,\mathrm{Na}^+} S_{\mathrm{NaCl}})$. From this we get $\eta_s^{m,\mathrm{pred}} = 1.08$ mV/K, lower than the seawater potential. The same tendency was observed by Kristiansen et al. [2], in a RED unit cell with brackish- and saltwater samples. This cannot be explained by extrapolation of results from the NaCl−$MgCl_2$ solutions, as we then would have expected a lower potential. There are however other ions present, and the NaCl−$MgCl_2$ system proved that small fractions of ions in the external solution can have a large impact on the ion composition in the membrane. A relevant ion in this regard is K^+, which yielded the highest Seebeck coefficients in the single-salt solution measurements. $m_{\mathrm{Na}^+}/m_{\mathrm{K}^+} = 0.019$, which is comparable with the concentration ratio of sodium and magnesium in the NaCl−$MgCl_2$ systems. The effect of K^+ could, therefore, be significant. This is in line with the selectivity order for competitive transport in CMX membranes by Chaabouni et al. [59], where the selectivity towards K^+ was higher than towards Ca^{2+} and Na^+. The same order has been found in Nafion membranes [63]. If this selectivity order is similar for the FKS-membrane, we could expect a significant contribution from K^+. This selectivity order is disputed, however [64, 65], and should be determined for the FKS-membranes used here.

$SO_4{}^{2-}$ ions are present in a relatively large amount in seawater and can have a significant effect on the thermoelectric potential in a unit cell of both a CEM and an AEM. The thermoelectric potential measurement here is with only a CEM, and $SO_4{}^{2-}$ is present as a co-ion. We can expect this co-ion-effect to be small, because of the ion's high valence charge, leading to exclusion from the membrane [7, 66].

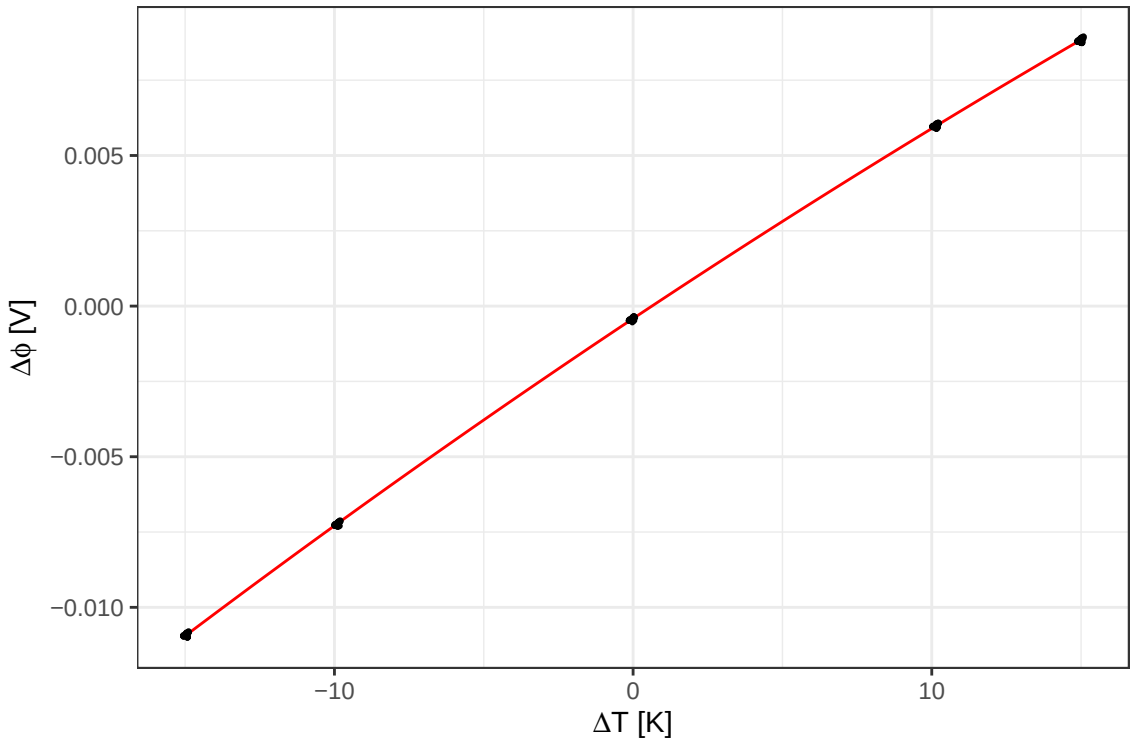

Figure 4.15: Measurements of cell potential plotted against the bulk tempeture difference with FKS-membranes in equilibrium with seawater. The red curve is the regression curve of eq. (4.29) fitted to the data.

4.3.4 Novel cellulose-based membranes

The thermoelectric potential was measured in two novel, cellulose-based membranes, following a similar procedure as for measurements with the commercial FKS membranes in single-salt solutions. In all cases, a linear relation between the cell voltage and the temperature difference was observed, and a linear model was fitted to the mean cell voltage and temperature difference at each temperature difference.

Table 4.8 shows the thermoelectric potential measured in membrane E and T, in combination with the different support materials. The results show that the thermoelectric potentials of the membranes in combination with filter support materials are marginally higher than the potential measured using only filter papers. This is likely due to that the majority of the temperature difference is not across the ion exchange membrane. In the case with four filter papers with a double layer of ion exchange membranes in the middle, the total thickness is approximately 0.48 mm, with the ion exchange membrane layer being 0.04 mm. We can do an order-of-magnitude analysis, assuming that the thermal conductivity of the filter paper and the ion-exchange membrane is equal. At steady-state, the temperature difference across only the ion-exchange membrane is proportional to its fraction of the total thickness of the membrane and the paper sheets. In the case with four filter papers with a double layer of ion exchange membranes in the middle, the total

thickness is approximately 0.48 mm, with the ion exchange membrane layer being approximately 0.04 mm. The temperature difference across the ion exchange membrane is then 8% of the total difference across the layers. Temperature polarization comes in addition, with increasing importance for thinner membranes.

The metal grids were employed to ensure that a larger fraction of the bulk temperature difference was across the membranes. The grid will affect the flow and a CFD analysis of this effect was not done, so the temperatures at the membranes were not estimated. But the Seebeck coefficients obtained in these measurements were close to those obtained with filter papers. This may still be due to that only a small fraction of the bulk temperature difference is across the membrane. Another explanation could be that the selectivity is low. To test this, a measurement at a concentration of 0.01 mol/kg NaCl was conducted, as the selectivity generally increases with a lower concentration [25].

The difference in the Seebeck coefficient obtained with membrane E and T is unsystematic. This could be due to small fractures in the membrane surfaces, especially membrane E was expected to be prone to this. Fractures in the membrane area in contact with the solution were not observed. However, this does not exclude the possibillity of smaller fractures. Another explanation could be that the membranes not had reached equilibrium with the external solution.

Estimated Seebeck coefficients in NaCl solutions are given in table 4.2. In 0.1 mol/kg NaCl the estimated Seebeck coefficient is 1.04 mV/K, and at 0.01 mol/kg, it is equal to 1.20 mol/kg. The Seebeck coefficient obtained here for 0.01 mol/kg is equal to that of the solution Seebeck coefficient, and for 0.1 mol/kg, it is slightly lower than the estimated solution Seebeck coefficient. We can conclude from this that the thermoelectric potentials measured here presumptively are dominated by unselective transport in the external solute and the filter papers.

Membrane	Support material	η_s^{obs} [mV/K]	Concentration [mol/kg]
E	4 paper filters	0.989 ± 0.002	0.1
T	4 paper filters	0.983 ± 0.002	0.1
-	4 paper filters	0.977 ± 0.003	0.1
T	2 paper filters	0.984 ± 0.002	0.1
E	Metal grid	0.957 ± 0.002	0.1
T	Metal grid	0.980 ± 0.002	0.1
T	Metal grid	1.201 ± 0.005	0.01

Table 4.8: Thermoelectric potential in cellulose-derived membranes immersed in NaCl solutions.

Chapter 5

Conclusion and further work

The scope of this thesis has been to better understand the Seebeck effect in ion-exchange membranes relevant for RED, by investigating the effect of ion species and of mixtures of ions experimentally. In a larger context, this is important for understanding how temperature gradients across ion exchange membranes in RED can be used to enhance the power production through the mixing of fresh- and seawater.

5.1 CFD analysis of the thermocell

Temperature polarization is temperature gradients in the solution instead of through the membrane, which may affect measurements of the thermoelectric potential across the membranes. Computational fluid dynamics was used to estimate temperature polarization in the thermocell used in the experimental sections of this thesis. According to the results, temperature polarization was present in the thermocell, and the temperature difference across the membrane was a constant fraction of the bulk temperature difference. This is valuable information when evaluating the results of the thermoelectric potential measurements. Some degree of temperature polarization was expected, but the results should preferentially be undergo further validation through experiments.

Softwares like Ansys Fluent provide powerful tools for evaluating various flow problems. In experiments that involve fluid flows, such tools should be considered in order to evaluate the experiments and reduce uncertainties. The tools could also serve to help designing experiments e.g. to reduce the effect of phenomena like temperature polarization.

5.2 The Seebeck effect in FKS-membranes in single-salt solutions

The Seebeck coefficient was measured in a stack of commercial Fumasep FKS-membranes in equilibrium with single-salt solutions of $CaCl_2$, $MgCl_2$, KCl and NaCl. The Seebeck coefficent varied as expected linearly with the logarithm of the activity of the external

electrolyte, and was generally higher for monovalent ions than divalent ions. In a further analysis of the performance between the ions, the quantity Λ_m was defined, which is independent of the concentration. This quantity showed a clear separation between the ions. Moreover, a correlation with the hydrated radius of the ions was observed. The nature of this correlation is unclear and should be further investigated, both theoretically and experimentally.

5.3 The Seebeck effect in FKS-membranes in NaCl−$MgCl_2$ systems

The Seebeck effect has been studied with mixtures of NaCl and $MgCl_2$ and systematically compared with pure NaCl. Even small amounts of Mg^{2+} had a significant, negative impact on the Seebeck coefficient. The change in the Seebeck coefficient following the addition of $MgCl_2$ can be attributed to a large $t_{Mg^{2+}}$ relative to the concentration in the external solution. Two different data analysis methods indicate this. A large $t_{Mg^{2+}}$ can, in turn, be explained by a higher membrane affinity towards Mg^{2+} than Na^+. This should be validated by experiments designed to measure the membrane composition and ion transport numbers directly.

In multi-ionic membrane transport, the ion exchange between ions in the membrane and the free solution determines the equilibrium composition of the membrane. In the presence of temperature gradients, however, the temperature dependence of the exchange process may affect the thermoelectric potential. This could give rise to concentration gradients in the membrane. How this affects the thermoelectric potential should be further investigated.

5.4 The Seebeck effect in FKS-membranes in seawater

Understanding the effects of mixed electrolytes on the Seebeck effect is a step on the way to understand the Seebeck effect in membrane systems with seawater and other natural feed solutions. A measurement of the Seebeck coefficient using seawater was therefore also conducted, and compared with results from the NaCl−$MgCl_2$ system. The Seebeck coefficient was, in this case, higher in pure NaCl at the corresponding concentration, which was unexpected. One explanation could be the presence of KCl. The Seebeck coefficient in KCl is higher than in NaCl at the same concentration, and the fraction of K^+ in seawater is comparable to the fraction of Mg^{2+} in the NaCl−$MgCl_2$ systems. Thus it is plausible that K^+ would have a positive effect on the potential. This hypothesis should be investigated, however.

The membrane Seebeck coefficient in a multi-ion system is determined by the ion transport

numbers, the water transport and the transported entropies of the ions. In this thesis, their combined effects are investigated. In order to properly separate their contributions, the water and ion transport numbers should be investigated as functions of the composition to accurately determine the nature of the transported entropies.

5.5 The Seebeck effect in novel cellulose membranes

The thermoelectric potential was measured in novel, cellulose-based membranes. The results were inconclusive with respect to the performance of the ion-exchange membranes, as the results indicated that the majority of the contribution to the thermoelectric potential came from the external solution. From the physical appearance of the membranes, however, we can conclude that the membranes were stable in up to 0.1 mol/kg NaCl, although a need for a support material was evident.

Further research should be devoted to developing new, cheap membranes, as the cost of currently available membranes limits the feasibility of RED. Cellulose could be a suitable raw material in this regard, as the raw material is abundant and obtained from renewable sources.

Bibliography

[1] M. Tedesco, A. Cipollina, A. Tamburini, and G. Micale. Towards 1kw power production in a reverse electrodialysis pilot plant with saline waters and concentrated brines. *Journal of Membrane Science*, 522:226 – 236, 2017.

[2] K. R. Kristiansen, V. M. Barragán, and S. Kjelstrup. Thermoelectric power of ion exchange membrane cells relevant to reverse electrodialysis plants. *Phys. Rev. Applied*, 11:044037, Apr 2019.

[3] G. Z. Ramon, B. J. Feinberg, and E. M. V. Hoek. Membrane-based production of salinity-gradient power. *Energy & environmental science*, 4(11):4423–4434, 2011.

[4] Y. Mei and C. Y. Tang. Recent developments and future perspectives of reverse electrodialysis technology: A review. *Desalination*, 425:156 – 174, 2018.

[5] J. W. Post, H. V.M. Hamelers, and C. J.N. Buisman. Influence of multivalent ions on power production from mixing salt and fresh water with a reverse electrodialysis system. *Journal of Membrane Science*, 330(1):65 – 72, 2009.

[6] T. Rijnaarts, E. Huerta, W. van Baak, and K. Nijmeijer. Effect of divalent cations on red performance and cation exchange membrane selection to enhance power densities. *Environmental Science & Technology*, 51(21):13028–13035, 2017. PMID: 28950057.

[7] D. A. Vermaas, J. Veerman, M. Saakes, and K. Nijmeijer. Influence of multivalent ions on renewable energy generation in reverse electrodialysis. *Energy Environ. Sci.*, 7:1434–1445, 2014.

[8] Z.-Y. Guo, Z.-Y. Ji, Y.-G. Zhang, F.-J. Yang, J. Liu, Y.-Y. Zhao, and J.-S. Yuan. Effect of ions (k+, mg2+, ca2+ and so42-) and temperature on energy generation performance of reverse electrodialysis stack. *Electrochimica Acta*, 290:282 – 290, 2018.

[9] M. Micari, A. Cipollina, F. Giacalone, G. Kosmadakis, M. Papapetrou, G. Zaragoza, G. Micale, and A. Tamburini. Towards the first proof of the concept of a reverse electrodialysis - membrane distillation heat engine. *Desalination*, 453:77 – 88, 2019.

[10] F. Giacalone, F. Vassallo, L. Griffin, M.C. Ferrari, G. Micale, F. Scargiali, A. Tamburini, and A. Cipollina. Thermolytic reverse electrodialysis heat engine: model development, integration and performance analysis. *Energy Conversion and Management*, 189:1 – 13, 2019.

[11] F. Giacalone, F. Vassallo, F. Scargiali, A. Tamburini, A. Cipollina, and G. Micale. The first operating thermolytic reverse electrodialysis heat engine. *Journal of Membrane Science*, 595:117522, 2020.

[12] A. M. Benneker, J. Klomp, R. G.H. Lammertink, and J. A. Wood. Influence of temperature gradients on mono- and divalent ion transport in electrodialysis at limiting currents. *Desalination*, 443:62 – 69, 2018.

[13] N. Lakshminarayanaiah. Transport phenomena in artificial membranes. *Chemical Reviews*, 65(5):491–565, 1965. PMID: 5318452.

[14] M. Tasaka, S. Morita, and M. Nagasawa. Membrane potential in nonisothermal systems. *The Journal of Physical Chemistry*, 69(12):4191–4197, 1965.

[15] M. Tasaka, K. Hanaoka, Y. Kurosawa, and C. Wada. Thermal membrane potential through charged membranes in electrolyte solutions. *Biophysical Chemistry*, 3(4):331 – 337, 1975.

[16] G. Scibona, C. Botré, F. Botré, and C. Fabiani. Nafion membrane potential in non-isothermal systems. *Electrochimica Acta*, 36(1):135 – 138, 1991.

[17] V.M. Barragán, K.R. Kristiansen, and S. Kjelstrup. Perspectives on thermoelectric energy conversion in ion-exchange membranes. *Entropy*, 20(12), 2018.

[18] L. Fu, L. Joly, and S. Merabia. Giant thermoelectric response of nanofluidic systems driven by water excess enthalpy. *Physical review letters*, 123(13):138001, 2019.

[19] J. Zhong and C. Huang. Thermal-driven ion transport in porous materials for thermoelectricity applications. *Langmuir*, 36(6):1418–1422, 2020.

[20] W. Zhang, Q. Wang, M. Zeng, and C. Zhao. Thermoelectric effect and temperature-gradient-driven electrokinetic flow of electrolyte solutions in charged nanocapillaries. *International Journal of Heat and Mass Transfer*, 143:118569, 2019.

[21] T. Li, X. Zhang, S. D. Lacey, R. Mi, X. Zhao, F. Jiang, J. Song, Z. Liu, G. Chen, J. Dai, et al. Cellulose ionic conductors with high differential thermal voltage for low-grade heat harvesting. *Nature materials*, 18(6):608–613, 2019.

[22] A. Daniilidis, R. Herber, and D.A. Vermaas. Upscale potential and financial feasibility of a reverse electrodialysis power plant. *Applied Energy*, 119:257–265, 2014. cited By 56.

[23] H. Farrokhzad, M. R. Moghbeli, T. Van Gerven, and B. Van der Bruggen. Surface modification of composite ion exchange membranes by polyaniline. *Reactive and Functional Polymers*, 86:161–167, 2015.

[24] Y. Mizutani. Ion exchange membranes with preferential permselectivity for monovalent ions. *Journal of membrane science*, 54(3):233–257, 1990.

[25] T. Luo, S. Abdu, and M. Wessling. Selectivity of ion exchange membranes: A review. *Journal of Membrane Science*, 555:429 – 454, 2018.

[26] T. Sata. *Ion exchange membranes preparation, characterization, modification and application*. Royal Society of Chemistry, Cambridge, 2004.

[27] O. S. Burheim. Thermal signature and thermal conductivities of pem fuel cells, 2009.

[28] A. H. Avci, T. Rijnaarts, E. Fontananova, G. [Di Profio], I. F.V. Vankelecom, W. M. [De Vos], and E. Curcio. Sulfonated polyethersulfone based cation exchange membranes for reverse electrodialysis under high salinity gradients. *Journal of Membrane Science*, 595:117585, 2020.

[29] X. Liu, M. He, D. Calvani, H. Qi, K. B. S. S. Gupta, H. J. M. de Groot, G. J. A. Sevink, F. Buda, U. Kaiser, and G. F. Schneider. Power generation by reverse electrodialysis in a single-layer nanoporous membrane made from core-rim polycyclic aromatic hydrocarbons. *Nature nanotechnology*, 2020.

[30] J. H. Jo, C.-H. Jo, Z. Qiu, H. Yashiro, L. Shi, Z. Wang, S. Yuan, and S.-T. Myung. Nature-derived cellulose-based composite separator for sodium-ion batteries. *Frontiers in Chemistry*, 8:153, 2020.

[31] N. Shaari and S. K. Kamarudin. Chitosan and alginate types of bio-membrane in fuel cell application: an overview. *Journal of Power Sources*, 289:71–80, 2015.

[32] S.A. Muhmed, N. A. M. Nor, J. Jaafar, A. F. Ismail, M.H.D. Othman, M. A. Rahman, F. Aziz, and N. Yusof. Emerging chitosan and cellulose green materials for ion exchange membrane fuel cell: a review. *Energy, Ecology and Environment*, pages 1–23, 2019.

[33] R.S.L. Yee, R.A. Rozendal, K. Zhang, and B.P. Ladewig. Cost effective cation exchange membranes: A review. *Chemical Engineering Research and Design*, 90(7):950 – 959, 2012.

[34] H. Vink and S.A.A. Chishti. Thermal osmosis in liquids. *Journal of Membrane Science*, 1(C):149–164, 1976. cited By 31.

[35] V.M. Barragán and C. Ruiz-Bauzá. Effect of unstirred solution layers on the thermal membrane potential through cation-exchange membranes. *Journal of Membrane Science*, 125(2):219 – 229, 1997.

[36] ANSYS Fluent. Ansys fluent theory guide 2019 r3. *Inc, Canonsburg, PA*, 2019.

[37] J. Tu, G. H. Yeoh, and C. Liu. *Computational Fluid Dynamics : A Practical Approach.*, volume 2nd ed. Butterworth-Heinemann, 2013.

[38] B. Andersson, R. Andersson, L. Håkansson, M. Mortensen, R. Sudiyo, and B. van Wachem. *Best practice guidelines*, page 174–180. Cambridge University Press, 2011.

[39] B. Kanargi, P. S. Lee, and C. Yap. A numerical and experimental investigation of heat transfer and fluid flow characteristics of an air-cooled oblique-finned heat sink. *International Journal of Heat and Mass Transfer*, 116:393 – 416, 2018.

[40] L. Yang, H. Han, Y. Li, and X. Li. A Numerical Study of the Flow and Heat Transfer Characteristics of Outward Convex Corrugated Tubes With Twisted-Tape Insert. *Journal of Heat Transfer*, 138(2), 09 2015. 024501.

[41] EW Lemmon, MO McLinden, DG Friend, P Linstrom, and W Mallard. Nist chemistry webbook, nist standard reference database number 69. *National Institute of Standards and Technology, Gaithersburg*, 2011.

[42] S. Kjelstrup and D. Bedeaux. *Non-equilibrium thermodynamics of heterogeneous systems*, volume 16. World Scientific, 2008.

[43] K. S. Førland and T. Førland. *Irreversible thermodynamics: theory and applications*. John Wiley & Sons Inc, 1988.

[44] T. Holt, S. K. Ratkje, K. S. Førland, and T. Østvold. Hydrostatic pressure gradients in ion exchange membranes during mass and charge transfer. *Journal of Membrane Science*, 9(1-2):69–82, 1981.

[45] P. Trivijitkasem and T. Østvold. Water transport in ion exchange membranes. *Electrochimica Acta*, 25(2):171 – 178, 1980. The 31st meeting of the International Society of Electrochemistry Held in Honour of Professor Grjotheim's 60th Birthday.

[46] S. K. Ratkje. Heat and internal energy changes at electrodes and junctions in thermocells. *Journal of The Electrochemical Society*, 137(7):2088, 1990.

[47] C. J. Petit, M. H. Hwang, and J. L. Lin. The soret effect in dilute aqueous alkaline earth and nickel chloride solutions at 25 °c. *International Journal of Thermophysics*, 7(3):687–697, 1986.

[48] J. Rumble and T.J. Bruno. *CRC Handbook of Chemistry and Physics 2019-2020: A Ready-reference Book of Chemical and Physical Data*. CRC Handbook of Chemistry and Physics. Taylor & Francis Group, 2019.

[49] K. S. Pitzer. *Molecular Structure And Statistical Thermodynamics: Selected Papers Of Kenneth S Pitzer*. Number vol. 1 in World Scientific Series in 20th Century Chemistry. World Scientific, 1993.

[50] L. F. Vekens, J. F. Zeeland, and J. Lin. Thermal diffusion studies with the Ag|AgCl|Cl^- electrode. *Journal of The Electrochemical Society*, 118(7):1119, 1971.

[51] A. Zlotorowicz, R. Strand, O. S. Burheim, Ø. Wilhelmsen, and S. Kjelstrup. The permselectivity and water transference number of ion exchange membranes in reverse electrodialysis. *Journal of Membrane Science*, 523:402–408, 2017.

[52] S. Zhu, R. S. Kingsbury, D. F. Call, and O. Coronell. Impact of solution composition on the resistance of ion exchange membranes. *Journal of Membrane Science*, 554:39–47, 2018.

[53] E. Fontananova, D. Messana, R. A. Tufa, I. Nicotera, V. Kosma, E. Curcio, W. Van Baak, E. Drioli, and G. Di Profio. Effect of solution concentration and composition on the electrochemical properties of ion exchange membranes for energy conversion. *Journal of Power Sources*, 340:282–293, 2017.

[54] E.R. Nightingale Jr. Phenomenological theory of ion solvation. effective radii of hydrated ions. *Journal of Physical Chemistry*, 63(9):1381–1387, 1959.

[55] A. C. Davison and D. V. Hinkley. *Bootstrap Methods and Their Application.*, volume Reprinted with corrections of *Cambridge Series on Statistical and Probabilistic Mathematics*. Cambridge University Press, 1999.

[56] A. Chapotot, G. Pourcelly, and C. Gavach. Transport competition between monovalent and divalent cations through cation-exchange membranes. exchange isotherms and kinetic concepts. *Journal of Membrane Science*, 96(3):167–181, 1994.

[57] V.I Zabolotsky, J.A Manzanares, V.V Nikonenko, K.A Lebedev, and E.G Lovtsov. Space charge effect on competitive ion transport through ion-exchange membranes. *Desalination*, 147(1-3):387–392, 2002.

[58] A.H. Galama, G. Daubaras, O.S. Burheim, H.H.M. Rijnaarts, and J.W. Post. Seawater electrodialysis with preferential removal of divalent ions. *Journal of Membrane Science*, 452:219 – 228, 2014.

[59] A. Chaabouni, F. Guesmi, I. Louati, C. Hannachi, and B. Hamrouni. Temperature effect on ion exchange equilibrium between cmx membrane and electrolytes solutions. *Journal of Water Reuse and Desalination*, 5(4):535–541, 12 2015. Copyright - Copyright IWA Publishing Dec 2015; Last updated - 2019-10-29.

[60] D. Muraviev, J. Noguerol, and M. Valiente. Separation and concentration of calcium and magnesium from sea water by carboxylic resins with temperature-induced selectivity. *Reactive and Functional Polymers*, 28(2):111 – 126, 1996. Proceedings of the 5th Spanish-Italian and Mediterranean Basin Congress.

[61] L. D. Talley, G. L. Pickard, W. J. Emery, and J. H. Swift. Chapter 3 - physical properties of seawater. In L. D. Talley, G. L. Pickard, W. J. Emery, and J. H. Swift, editors, *Descriptive Physical Oceanography (Sixth Edition)*, pages 29 – 65. Academic Press, Boston, sixth edition edition, 2011.

[62] A. G. Dickson and C. Goyet. Handbook of methods for the analysis of the various parameters of the carbon dioxide system in sea water. version 2. Technical report, Oak Ridge National Lab., TN (United States), 1994.

[63] M. J. Manning and S. S. Melsheimer. Binary and ternary ion-exchange equilibriums with a perfluorosulfonic acid membrane. *Industrial & Engineering Chemistry Fundamentals*, 22(3):311–317, 1983.

[64] A. H. Avci, R. A. Tufa, E. Fontananova, G. Di Profio, and E. Curcio. Reverse electrodialysis for energy production from natural river water and seawater. *Energy*, 165:512–521, 2018.

[65] B. S. Vo and D. C. Shallcross. Ion exchange equilibria data for systems involving h+, na+, k+, mg2+, and ca2+ ions. *Journal of Chemical & Engineering Data*, 50(3):1018–1029, 2005.

[66] M. Higa, A. Tanioka, and K. Miyasaka. At study of ion permeation across a charged membrane in multicomponent ion systems as a function of membrane charge density. *Journal of Membrane Science*, 49(2):145 – 169, 1990.

[67] V. M. M Lobo. Handbook of electrolyte solutions : A and b, 1989.

Nomenclature

Symbol	Description	Units
a_i	Chemical activity	-
c	Fraction of the bulk temperature difference across the membrane	-
ϵ	molal concentration ratio of Mg^{2+} and Na^{+}	-
η_s	Seebeck coefficient	V/K
F	Faraday constant	C/mol
F_b	Body forces	N
g	gravity	m/s^2
$\gamma_{\pm}$	Mean eletrolyte activity coefficient	mol^{-1}
γ_i	single ion activity coefficient	$mol^{-\nu_i}$
h_i	Specific enthalpy	kJ/kg
h	Heat transfer coefficient	$W/m^{-2}s^{-1}$
j	Current density	A/m^2
J_i	Component mass flux density	mol/(m^2 s)
J'_q	Measurable heat flux density	J/(m^2 s)
k	Thermal conductivity	Pa
L_{ij}	Onsager phenomenological coefficients	
l_m	Membrane thickness	m
m	Molality	mol/kg solute
μ_i	Chemical potential	kJ/mol
ν	Stoichiometric constant of ion dissociation	-

p	Pressure	Pa
ϕ	Electromotive potential	V
Π	Peltier heat	
R	Universal gas constant	J/(K mol)
ρ	Density	kg/m^3
$c_{p,i}$	Partial molar heat capacity	J/(K mol)
S_i^*	Transported entropy in membrane	J/(K mol)
$S_i^{*,sol}$	Transported entropy in the solution	J/(K mol)
S_h	Energy source term	kW
S_i	Partial molar entropy	J/(K mol)
σ	Entropy production density	J/(K mol m^3 s)
T	Temperature	K
t_i	Dimensionless transport number in membrane	-
t_i^{sol}	Dimensionless transport number in solution	-
τ_i	Thomson coefficient	mV/K
τ^s	Shear stress	Pa
v	Velocity	m/s
y^+	Dimensionless distance from wall	-

List of Figures

List of Tables

Appendix A

Computer aided drawing (CAD) of the experimental cell

Figure A.1 shows the model of the fluid in the flowchamber, created with the Solidworks software. Voids for the thermocouple and electrode are marked. Figure A.2 shows the fully assembled model of the thermocell.

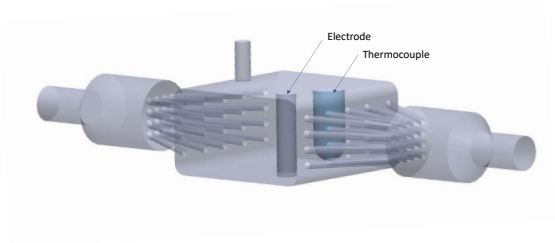

Figure A.1: Solidworks CAD model of the flowchamber

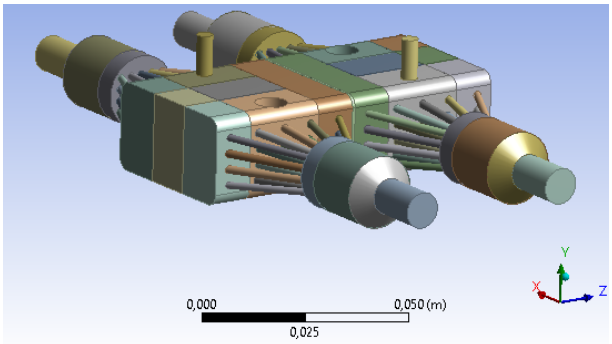

Figure A.2: Fully assembled and partitioned model in Ansys designmodeler.

Appendix B

Activity coefficients from the Pitzer equations

The pitzer equations were derived by K. S. Pitzer [49] for calculating activity coefficients in various electrolytes. They are derived from a virial expansion of the excess Gibbs free energy of solutions and give a set of equations that give the activity coefficients in multicomponent electrolytes with high accuracy. The equations are therefore suitable to calculate the activity coefficients in a binary solution of NaCl and $MgCl_2$. The equations depend on both interaction parameters between ions of the opposite charge and between ions of the same charge. While the latter is necessary in concentrated electrolytes, experiments have shown that interactions between ions of the opposite charge will dominate in dilute systems. For NaCl, the activity coefficient is

$$\begin{aligned}\ln\gamma_{\mathrm{NaCl}} = f^{\gamma} + (m_{\mathrm{Na^+}} + m_{\mathrm{Cl^-}})(B_{\mathrm{NaCl}} + m_{\mathrm{Cl^-}}C_{\mathrm{NaCl}}) + m_{\mathrm{Mg^{2+}}}(B_{\mathrm{MgCl}}m_{\mathrm{Cl^-}} + C_{\mathrm{MgCl}}) \\ + m_{\mathrm{Na^+}}m_{\mathrm{Cl^-}}(B'_{\mathrm{NaCl}} + C_{\mathrm{NaCl}}) + m_{\mathrm{Mg^{2+}}}m_{\mathrm{Cl^-}}(B'_{\mathrm{MgCl}} + C_{\mathrm{MgCl}})\end{aligned} \tag{B.1}$$

While the $MgCl_2$ activity coefficient is

$$\begin{aligned}\ln\gamma_{\mathrm{MgCl_2}} = \frac{4}{3}\ln\gamma_{\mathrm{NaCl}} - \frac{1}{3}(-2f^{\gamma} + 2m_{\mathrm{Cl^-}}[2B_{\mathrm{NaCl}} - B_{\mathrm{MgCl}} \\ + (m_{\mathrm{Na^+}} + m_{\mathrm{Mg^{2+}}} + m_{\mathrm{Cl^-}})(2C_{\mathrm{NaCl}} - C_{\mathrm{MgCl}})] + m_{\mathrm{Mg^{2+}}}m_{\mathrm{Cl^-}}(-B'_{\mathrm{MgCl}}))\end{aligned} \tag{B.2}$$

Where f^{γ} is constant with respect to the ions, B_{ij} is the first virial coefficient describing interactions between ion i and j, and B'_{ij} is it's derivative with respect to the ion strength. C_{ij} is the second virial coefficient. In a solution of NaCl and $MgCl_2$, these quantities:

$$f^{\gamma} = -A^{\phi}\left(\frac{I^{1/2}}{1 + bI^{1/2}} + \frac{2}{b}(1 + bI^{1/2})\right) \tag{B.3}$$

$$B_{ij} = \beta_{ij}^{(0)} + \frac{2\beta_{ij}^{(1)}}{\alpha^2 I}\left[1 - (1 + \alpha I^{1/2})\exp(-\alpha I^{1/2})\right] \tag{B.4}$$

$$B'_{ij} = \frac{2\beta_{ij}^{(1)}}{\alpha^2 I^2}\left[1 - (1 + \alpha I^{1/2} + \frac{1}{2}\alpha^2 I)\exp(-\alpha I^{1/2})\right] \tag{B.5}$$

$$C_{ij} = \frac{3}{2}C_{ij}^{\phi} \tag{B.6}$$

Where I is the ionic strength. The other variables are empirical parameters, and their values are given in table B.1.

The Pitzer equations can also be used for single-salt solutions, in this case the expression for $\ln\gamma$ is

$$\ln\gamma = |z_+ z_-| f^\gamma + m\left(\frac{2\nu_+\nu_-}{\nu}\right) B_{ij} + m^2 \frac{(\nu_+\nu_-)^{3/2}}{\nu} C_{ij} \tag{B.7}$$

Where $\nu = \nu_- + \nu_+$ are the stoiciometric coefficients of ion dissociation, and z_+ and z_- is the valence charge of the cation and the anion respectively. A comparison of th Pitzer activity coefficients in single-salt solutions litterature values of the activity coefficients is shown in figure B.1. The coefficients agree well for all electrolytes considered.

Parameter	value	unit
A^ϕ	0.392	$(\mathrm{kg/mol})^{1/2}$
b	1.2	$(\mathrm{kg/mol})^{1/2}$
α	2.0	$(\mathrm{kg/mol})^{1/2}$
$\beta^{(0)}_{\mathrm{NaCl}}$	0.0765	$(\mathrm{kg/mol})^{1/2}$
$\beta^{(0)}_{\mathrm{KCl}}$	0.04835	kg/mol
$\beta^{(0)}_{\mathrm{MgCl}}$	0.35235	kg/mol
$\beta^{(0)}_{\mathrm{CaCl}}$	0.31592	kg/mol
$\beta^{(1)}_{\mathrm{NaCl}}$	0.2664	kg/mol
$\beta^{(1)}_{\mathrm{MgCl}}$	0.2122	kg/mol
$\beta^{(1)}_{\mathrm{MgCl}}$	1.6815	kg/mol
$\beta^{(1)}_{\mathrm{CaCl}}$	1.614	kg/mol
C^ϕ_{NaCl}	0.00127	$(\mathrm{kg/mol})^2$
C^ϕ_{KCl}	-0.00084	$(\mathrm{kg/mol})^2$
C^ϕ_{MgCl}	0.0104	$(\mathrm{kg/mol})^2$
C^ϕ_{CaCl}	-0.000679	$(\mathrm{kg/mol})^2$

Table B.1: Values of empirical parameters used in the Pitzer equations.

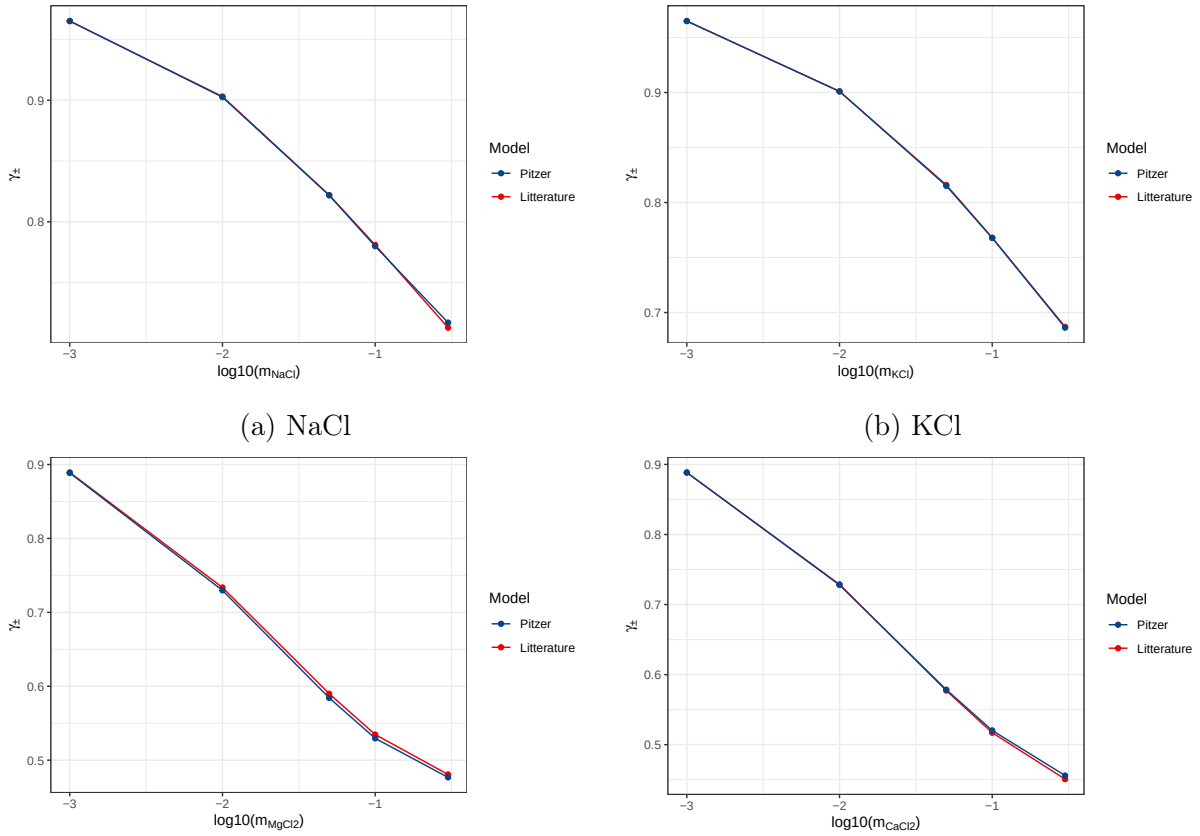

(a) NaCl (b) KCl

(c) $MgCl_2$ (d) $CaCl_2$

Figure B.1: Activity coefficients from the litterature [67], compared with coefficients calculated with Pitzer's equations, for single-salt electrolytes at relevant concentrations.

Appendix C

Uncorrected membrane Seebeck coefficients

Table C.1 shows membrane Seebeck coefficients in the single-salt solutions, with temperature polarization being neglected. The coefficients are thus related to the measured thermoelectric potential by the equation $(\Delta\phi/\Delta T)_{j=0} = \eta_s^m + \eta_s^{\mathrm{el}}$.

molality [mol/kg]	$\eta_{\mathrm{NaCl}}^{\mathrm{mem}}$ [mV/K]	$\eta_{\mathrm{KCl}}^{\mathrm{mem}}$ [mV/K]	$\eta_{\mathrm{MgCl_2}}^{\mathrm{mem}}$ [mV/K]	$\eta_{\mathrm{CaCl_2}}^{\mathrm{mem}}$ [mV/K]
0.3	-	1.173 ±0.007	0.975 ± 0.004	0.954 ± 0.006
0.1	1.207 ± 0.007	1.32 ± 0.01	1.084 ± 0.007	1.057 ± 0.006
0.05	-	1.423 ± 0.008	1.12 ± 0.01	1.118 ± 0.005
0.025	1.406 ± 0.009	-	-	-
0.01	1.563 ± 0.007	1.636 ± 0.009	1.226 ± 0.008	1.229 ± 0.007
0.005	1.632 ± 0.009	-	-	-
0.001	1.87 ± 0.03	1.99 ± 0.02	1.445 ± 0.008	1.485 ± 0.009

Table C.1: Estimated membrane Seebeck effect from measurement series with 10 FKS membranes, with temperature polarization neglected.

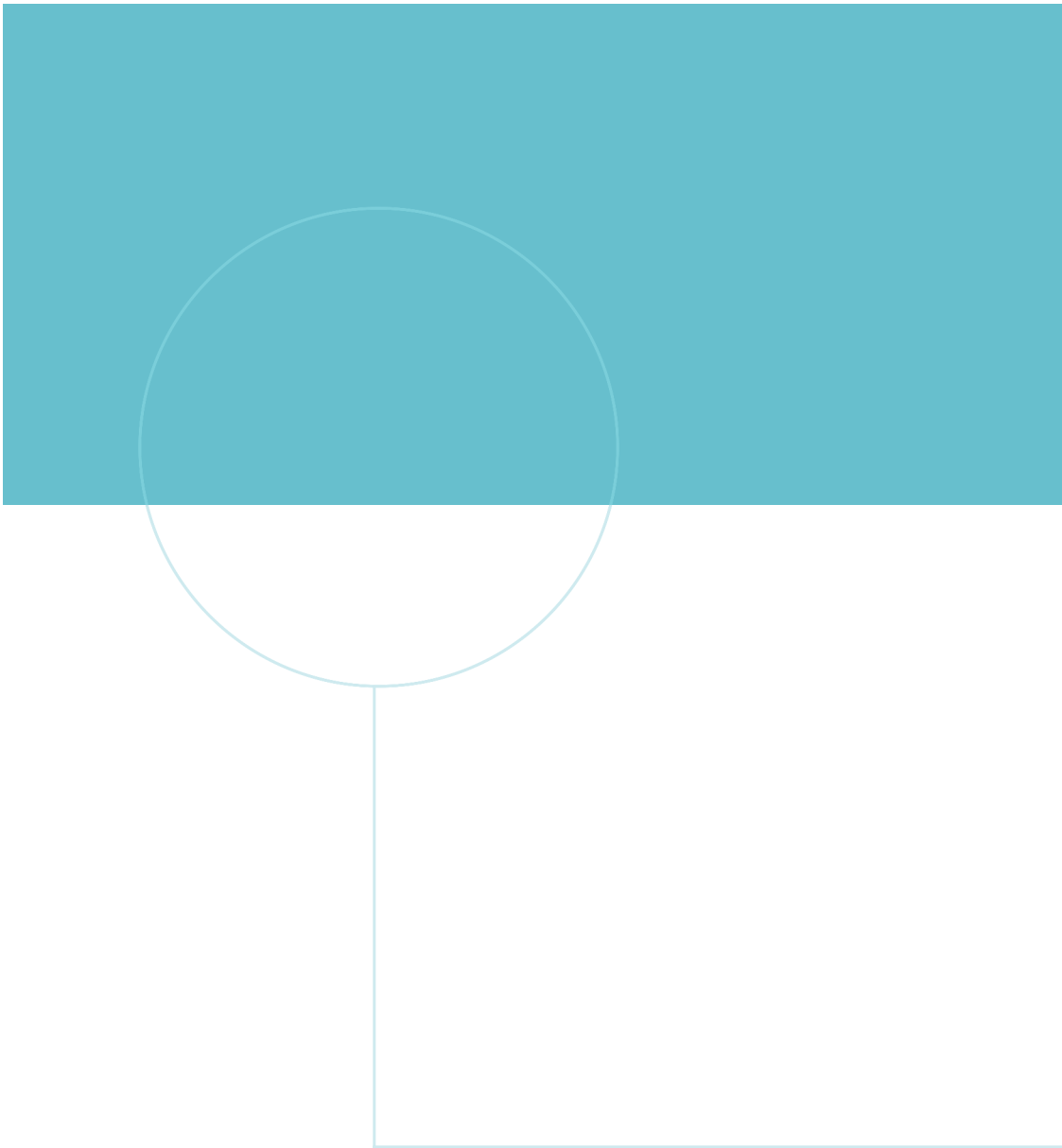

NTNU

Norwegian University of
Science and Technology